Biology of Reproduction, 2026, **115(4)**, 1331–1350
https://doi.org/10.1093/biolre/ioag185
Advance access publication date 31 August 2026
Research Article

LncRNA *THOR* regulates spermatogenesis by interacting with and stabilizing Sycp3 protein in zebrafish†

Jiayi Zhao[1,2,‡], Chaolin Jiang[1,3,‡], Yiran Luo[1,2], Xing Lin[1,4], Yifan Bai[1,2], Kaifeng Meng[1,5], Yuanli Zhao[1,5], Fei Liu[1,2,*] and Daji Luo[1,2,5,*]

[1]State Key Laboratory of Breeding Biotechnology and Sustainable Aquaculture, Institute of Hydrobiology, Chinese Academy of Sciences, Wuhan, China
[2]College of Advanced Agricultural Sciences, University of Chinese Academy of Sciences, Beijing, China
[3]State Key Laboratory of Developmental Biology of Freshwater Fish, Hunan Normal University, Changsha, China
[4]College of Advanced Agricultural Sciences, Zhejiang Wanli University, Ningbo, China
[5]College of Fisheries, Guangdong Ocean University, Zhanjiang, China

*__Correspondence:__ Fei Liu, State Key Laboratory of Breeding Biotechnology and Sustainable Aquaculture, Institute of Hydrobiology, Chinese Academy of Sciences, Wuhan 430072, China. E-mail: liufei2018@ihb.ac.cn, Tel: +86 13554697245; Daji Luo, College of Advanced Agricultural Sciences, University of Chinese Academy of Sciences, Beijing 100049, China. E-mail: luodaji@ihb.ac.cn, Tel: +86 19075777067

†__Grant Support:__ This work was supported by the National Natural Science Foundation of China (Grant No. 32425055 and 32630109), the Innovation Team Project of the State Key Laboratory of Breeding Biotechnology and Sustainable Aquaculture (2024BBSA01), and the Foundation of Hubei Hongshan Laboratory (2022hszd022).

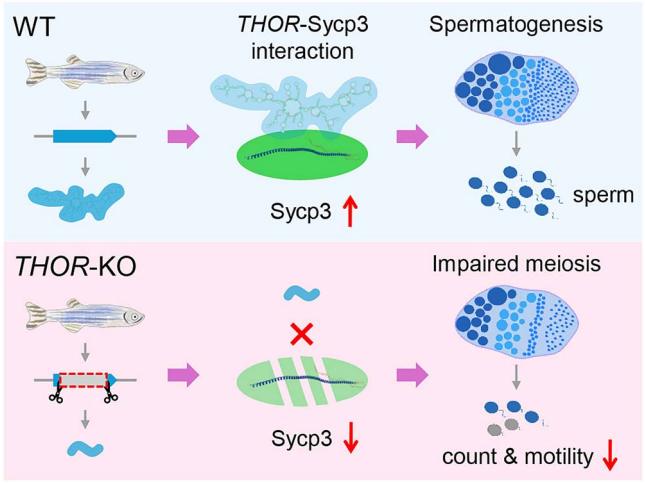
‡Jiayi Zhao and Chaolin Jiang contributed equally to this work.

Abstract

Testis-associated highly conserved oncogenic long non-coding RNA (*THOR*) is a highly conserved and testis-enriched long non-coding RNA (lncRNA) across vertebrates that plays diverse roles in various cancers. However, its physiological function and regulatory mechanism in testes remain largely unknown. Here, we investigated the genomic location and expression pattern of *THOR* in the model organism zebrafish, and generated a homozygous *THOR* knockout model using clustered regularly interspaced palindromic repeats (CRISPR)-Cas9 technology. Loss of *THOR* in zebrafish impaired spermatogenesis, leading to oligospermia (38.7% reduction in sperm count), reduced sperm motility, sperm ultrastructural defects, and decreased fertilization rates. RNA sequencing (RNA-seq) analysis of wild type (WT) and *THOR* knockout testes revealed dysregulation of cell cycle-related genes, including *cyclin-dependent kinase inhibitor 1D* (*cdkn1d*), *forkhead box O1 a* (*foxo1a*), *TSC complex subunit 1a* (*tsc1a*), *TSC complex subunit 2* (*tsc2*), *ATRX chromatin remodeler* (*atrx*), and *RAD21 cohesin complex component b* (*rad21b*). RNA pulldown assays in zebrafish testes identified 486 potential *THOR*-interacting proteins primarily involved in ribosome biogenesis, RNA splicing, chromatin architecture, and meiotic progression. Notably, the core synaptonemal complex components synaptonemal complex protein 1 (Sycp1), synaptonemal complex protein 2 (Sycp2), and synaptonemal complex protein 3 (Sycp3) were all captured as *THOR*-binding partners. We further demonstrated that *THOR* directly interacts with Sycp3 and positively regulates its protein levels. Immunostaining assays on chromosome spreads revealed a significantly higher frequency of discontinuous Sycp3 signals in $THOR^{-/-}$ testes, suggesting the presence of meiosis defects caused by Sycp3 downregulation. Our findings expand the understanding of lncRNA-mediated control of spermatogenesis and male infertility by providing the first evidence that lncRNA *THOR* interacts with the synaptonemal complex to regulate meiosis progression.

Received: May 14, 2026. **Revised:** August 11, 2026. **Accepted:** August 24, 2026
© The Author(s) 2026. Published by Oxford University Press on behalf of the Society for the Study of Reproduction.
This is an Open Access article distributed under the terms of the Creative Commons Attribution-NonCommercial License (https://creativecommons.org/licenses/by-nc/4.0/), which permits non-commercial re-use, distribution, and reproduction in any medium, provided the original work is properly cited. For commercial re-use, please contact reprints@oup.com for reprints and translation rights for reprints. All other permissions can be obtained through our RightsLink service via the Permissions link on the article page on our site—for further information please contact journals.permissions@oup.com.

Graphical Abstract



Summary Sentence

Knockout of long non-coding RNA testis-associated highly conserved oncogenic long non-coding RNA (*THOR*) in zebrafish causes oligospermia, reduced sperm motility, and decreased fertilization rates, via mechanisms involving dysregulated expression of cell cycle-related genes and a direct interaction between *THOR* and Sycp3.

Key words: spermatogenesis, lncRNA, *THOR*, Sycp3, synaptonemal complex, meiosis, male infertility

Introduction

Infertility is a widespread condition affecting about 15% of childbearing-age couples, and the percentage of infertile men has been estimated to range from 2.5% to 12% [1]. Spermatogenesis is a precisely coordinated developmental process comprising the sequential proliferation and differentiation of germ cells from spermatogonial stem cells into mature spermatozoa [2, 3]. Many factors, including genetic and epigenetic factors, endocrine dysfunction, lifestyle factors, gonadotoxic exposures, and aging, have been reported to disrupt the spermatogenesis process, resulting in infertility or reduced fertility in men [1, 4]. While the importance of spermatogenesis has been well recognized, the molecular architecture underlying this complex process remains largely unknown.

Long non-coding RNAs (lncRNAs) are defined as transcripts longer than 200 nucleotides with limited or no protein-coding capacity. Transcriptome studies in mammals have revealed that the testis expresses the highest number of lncRNAs, the majority of which are testis-specific [5–7], implying their potential roles in testicular physiology. Recent studies have provided increasing evidence for diverse functions of lncRNAs in spermatogenesis and male infertility [7–13]. For instance, the testis-specific lncRNA *Tscl1* has been reported to directly bind the PIWIL1 (piwi-like RNA-mediated gene silencing 1)/eIF3f (eukaryotic translation initiation factor 3, subunit F)/HuR (ELAV like RNA binding protein 1)/eukaryotic translation initiation factor 4 gamma 3 (eIF4G3) complex to regulate the translation of fatty-acid-metabolism-related messenger RNA (mRNAs), and knockout of *Tscl1* in mice caused complete male infertility [10]. Additionally, Pirmy and Pirmy-like lncRNAs, derived from the long arm of the mouse Y chromosome, serve as templates for Piwi-interacting RNA (piRNA) biogenesis and modulate the expression of key autosomal genes involved in spermatogenesis [12]. Despite these advances, the functions and regulatory mechanisms of the vast majority of testis-specific lncRNAs in spermatogenesis remain unexplored.

The lncRNA *THOR* (testis-associated highly conserved oncogenic long non-coding RNA) was originally identified as an ultraconserved lncRNA with the highest expression in normal testicular tissue and significantly elevated levels in various tumor cells [14, 15]. The roles and regulatory mechanisms of *THOR* in promoting tumor progression have been extensively studied [14, 16–19]. Several *THOR*-interacting proteins, including insulin like growth factor 2 mRNA binding protein 1 (IGF2BP1) [14, 18], heterogeneous nuclear ribonucleoprotein D (hnRNPD) [16], and Yes1 associated transcriptional regulator (YAP) [20], have been shown to mediate its oncogenic functions. Additionally, *THOR* stabilizes multiple mRNAs, such as *IGF2BP1* [14, 17], *catenin beta 1* (*CTNNB1*) [21, 22], and *SRY-box transcription factor 9* (*SOX9*) [19]. Beyond its oncogenic activities, *THOR* disruption in both zebrafish [14] and mice [23] leads to reduced male fertility, suggesting an evolutionarily conserved role of *THOR* in male reproduction. However, it remains unknown whether *THOR* employs the same molecular mechanisms in the testis as it does in tumor cells.

To investigate the testis-specific functions and regulatory mechanisms of *THOR*, we generated a *THOR* knockout zebrafish model using clustered regularly interspaced palindromic repeats (CRISPR)-Cas9 technology. We systematically examined male fertility parameters, including testicular morphology, sperm motility, fertilization rates, and expression of spermatogenesis-related genes. Furthermore, by combining RNA sequencing (RNA-seq) and RNA pulldown assays, we analyzed transcriptome-wide gene expression changes and identified potential *THOR*-interacting proteins in zebrafish testes. Our findings reveal a novel regulatory mechanism of

THOR in spermatogenesis that is distinct from its known roles in tumorigenesis.

Materials and methods

Animals

Wild-type AB strain zebrafish were obtained from the China Zebrafish Resource Center (CZRC). Zebrafish were maintained in a recirculating aquaculture system at a constant temperature of 28.5°C under a 14-h light/10-h dark photoperiod. Fish were fed twice daily with brine shrimp nauplii. All experimental procedures involving zebrafish were approved by the Institutional Animal Care and Use Committee of the Institute of Hydrobiology, Chinese Academy of Sciences.

Generation of *THOR* knockout zebrafish by CRISPR-Cas9

Two single-guide RNA (sgRNAs) spanning the conserved region of zebrafish *THOR* were designed using the CHOPCHOP webtool (http://chopchop.cbu.uib.no/). Primers used for amplifying DNA templates for sgRNA in vitro transcription are listed in Supplementary Table S1. In vitro transcription was performed using the T7 High Yield RNA Transcription Kit (TR101, Vazyme, Nanjing, China) according to the manufacturer's manual. A mixture of Cas9 protein (300 ng/μL) and pooled sgRNAs (200 ng/μL) was injected into one-cell-stage zebrafish embryos at a volume of 1 nL. Deletion of the conserved region of *THOR* was detected by polymerase chain reaction (PCR) and Sanger sequencing using genomic DNA samples from injected embryos at 45 hpf. Positive zebrafish embryos were raised to adulthood and propagated. After three generations of screening, a genetically stable *THOR* homozygous knockout line was obtained.

Cell culture

HEK293T cells (GDC0187, China Center for Type Culture Collection, Wuhan, China) were cultured in Dulbecco's modified Eagle medium (DMEM) (G4524, Servicebio, Wuhan, China) supplemented with 10% fetal bovine serum (G8003, Servicebio, Wuhan, China) and 1% penicillin–streptomycin (G4003, Servicebio, Wuhan, China). Cells were cultured at 37°C in a humidified incubator under 5% CO_2. Under light microscopy, cells exhibited normal morphology consistent with the typical phenotype of HEK293T cells. All cells were regularly tested for mycoplasma, bacterial, and fungal contamination and confirmed to be negative.

Plasmid construction and transfection

Zebrafish *THOR* was amplified from testis complementary DNA (cDNA) samples according to a previous study [14], and subcloned into the pcDNA3.1 vector. The coding sequence of zebrafish *sycp3* (ZDB-GENE-040910-2) was amplified and subcloned into the pCMV-3 × Flag vector. All constructs were confirmed by DNA sequencing. Cell transfection was performed using the Chemi-Trans Polyfectin DNA Transfection Reagent (T001, GeneCodeX, Wuhan, China) according to the manufacturer's instructions.

RNA isolation, reverse transcription, and quantitative PCR

Total RNA was extracted from zebrafish tissues and HEK293T cells using TransZol Up (ET111, TransGen, Beijing, China) according to the manufacturer's instructions. RNA concentration and purity were determined with a Nanodrop One spectrophotometer (Thermo Fisher Scientific). RNA integrity was verified by 1.2% agarose gel electrophoresis. First-strand cDNA was synthesized from 1 μg of total RNA using the EasyScript One-Step genomic DNA (gDNA) Removal and cDNA Synthesis SuperMix (AE311, TransGen, Beijing, China). Quantitative PCR (qPCR) was performed in 20 μL reaction volumes in biological and technical triplicate using the PerfectStart Green qPCR SuperMix (AQ601, TransGen, Beijing, China) on the CFX96 Touch Real-Time PCR Detection System (Bio-Rad). The amplification protocol consisted of an initial denaturation at 95°C for 30 s, followed by 40 cycles of 95°C for 5 s and 60°C for 30 s. Dissociation curve analysis was conducted to confirm amplification specificity. Relative gene expression was calculated using the $2^{-\Delta\Delta Ct}$ method with *eef1a1l1a* serving as an internal reference gene.

Histological analysis of zebrafish testis sections

After being fixed in 4% paraformaldehyde (PFA) in phosphate-buffered saline (PBS) at 4°C overnight, zebrafish testes were dehydrated in a graded ethanol series, permeabilized with xylene, embedded in paraffin, and then cut into 4 μm sections. To ensure consistent anatomical positioning across all slides, testis paraffin blocks from both wild type (WT) and $THOR^{-/-}$ zebrafish were trimmed to the largest central cross-section prior to sectioning. The sections were dewaxed in xylene, rehydrated through a graded ethanol series, and rinsed in distilled water. Hematoxylin and eosin staining (E607318, BBI, Shanghai, China) was performed according to the manufacturer's manual. Images were collected by an automatic digital slide scanner (SQS-40P, TEKSQRAY, Shenzhen, China).

Zebrafish sperm motility analysis

Sperm were collected from age-matched WT and $THOR^{-/-}$ zebrafish. Zebrafish sperm were diluted in Hanks solution (G4204, Servicebio, Wuhan, China) and temporarily stored on ice until analysis. Computer-assisted sperm analysis (CASA) was performed on the CEROS II sperm analysis system (Hamilton Thorne, Beverly, USA). For sperm motility assessment, 0.5 μL of sperm suspension was placed on a glass slide, and 1 μL of aerated water was added and mixed immediately. Sperm movement was recorded within the first 30 s, and motion parameters were analyzed accordingly.

Ultrastructural analysis of zebrafish sperm

Semen samples collected from WT and $THOR^{-/-}$ zebrafish were fixed overnight at 4°C in 2.5% glutaraldehyde. Fixed sperm were smeared onto glass slides and air-dried at room temperature. Dehydration was performed through a graded ethanol series (30%, 50%, 70%, 90%, 95%, and 100% ethanol) for 15 min at each concentration. Samples were then dried overnight in a desiccator, sputter-coated with gold, and imaged using a scanning electron microscope (S-4800, Hitachi, Japan).

Western blot

Zebrafish testes were homogenized in the radio immunoprecipitation assay (RIPA) Lysis Buffer (Beyotime, Cat: P0013B, Shanghai, China) containing protease inhibitors. Cultured cells were lysed in the same buffer on ice for 15 min, and

the lysates were collected with a cell scraper. Protein lysates were mixed with 5× loading buffer, boiled at 95°C for 5 min, and stored at −80°C prior to use. Protein samples were separated by sodium dodecyl sulfate-polyacrylamide gel electrophoresis (SDS-PAGE) and transferred to polyvinylidene fluoride (PVDF) membranes. The membranes were blocked in 5% skim milk dissolved in tris-buffered saline with tween 20 (TBST) buffer (20 mM Tris–HCl, 150 mM NaCl, 0.05% Tween 20, pH 7.6) for 1 h. The primary antibody solution was added and incubated overnight at 4°C. The following antibodies were used in this study: anti-zebrafish Sycp3 (CZPA3, China Zebrafish Resource Center), anti-zebrafish Sycp1 (customized, Frdbio, Wuhan, China), anti-alpha-tubulin (66031-1-Ig, Proteintech, Wuhan, China), and anti-FLAG antibody (M185-3 L, MBL, Japan). The membranes were washed three times in TBST for 5 min each and incubated in horseradish peroxidase (HRP)-conjugated secondary antibodies (111-035-003 and 115-035-003; Jackson ImmunoResearch Laboratories, West Grove, USA) for 2 h. After three washes (5 min each) in TBST, the signals were detected using the SuperSignal West Pico PLUS kit (34 580, Thermo Fisher Scientific) on the ImageQuant LAS 4000 mini system (GE Healthcare, Chicago, USA).

Tissue immunofluorescence staining

Zebrafish testes were fixed in 4% PFA at 4°C for 12–24 h. Cryosections were prepared according to previous studies [24, 25]. Antigen retrieval was performed by heating the slides in Tris-ethylenediaminetetraacetic acid (EDTA) buffer (10 mM Tris, 1 mM EDTA, 0.1% Tween-20, pH 9.0) at 95–100°C for 20 min, followed by cooling to room temperature for 1–2 h. Slides were washed three times in phosphate-buffered saline with Triton X-100 (PBST) (0.1%) for 5 min each on a horizontal shaker, blocked with 5% bovine serum albumin (BSA) in PBST for 30 min at room temperature, and incubated overnight at 4°C with the primary antibody solution. Slides were washed 5 min in PBST for three times and incubated with the secondary antibody solution for 2 h at room temperature in the dark. The following antibodies were used in this study: anti-zebrafish Sycp3 antibody (CZPA3, China Zebrafish Resource Center, 1:500 dilution), Phospho-Histone H3-S10 Rabbit mAb (AP1586, ABclonal, 1:500 dilution), and CoraLite488-conjugated Goat Anti-Rabbit IgG (SA00013-2, Proteintech, 1:1000 dilution). Nuclei were stained with 4',6-diamidino-2-phenylindole (DAPI) (28718-90-3, Biosharp, 5 μg/mL) for 5 min. Following final washes in PBST for three times, sections were mounted with anti-fade medium (01100079, Biosharp) and stored at 4°C in the dark until imaging with a confocal microscope (TCS SP8 DLS, Leica). The criteria for distinguishing between different meiotic stages of spermatocytes on a zebrafish testis section were adopted from a previous study [26], primarily based on the characteristic patterns of Sycp3 fluorescence signals.

Chromosome spread preparation

Four to six anesthetized male zebrafish were sacrificed, and intact testes were dissected and placed in ice-cold PBS. The testicular tissues were thoroughly minced to release spermatogenic cells, and the cell suspension was filtered through a 40 μm cell strainer to remove tissue debris. The filtered cell suspension was mixed with more than three volumes of 0.075 M KCl solution and incubated at 37°C for 90 min for hypotonic treatment. The suspension was gently inverted every several minutes throughout the hypotonic incubation to prevent cell aggregation. After hypotonic permeabilization, one-fourth volume of 4% PFA was added and fully mixed for cell fixation. Aliquots of 50–100 μL cell suspension were evenly spread onto positively charged glass slides and air-dried thoroughly in a ventilated hood. Cell suspensions were then spread onto slides, air-dried, and either stored at −20°C or processed immediately for immunostaining.

Chromosome spread immunostaining

The slides were boiled in preheated EDTA antigen retrieval solution for 25 min and cooled naturally. Subsequently, the slides were permeabilized with PBS containing 0.1% Tween 20 and 0.1% Triton X-100 for 10 min, followed by 10 min of room-temperature blocking with blocking buffer (10% goat serum, 3% BSA, 0.05% Triton X-100 in PBS). The anti-Sycp1 antibody (1:200 dilution) was validated and described in a previous study [27]. Primary antibody solutions against Sycp1 and Sycp3 were added and incubated on the slides overnight at 4°C in a humidified chamber. After three washes, the slides were incubated with fluorescently labeled secondary antibodies (1:500) and DAPI (5 μg/mL) for 1 h at 37°C in the dark. The slides were washed three times (10 min each) with PBS containing 0.04% Photo-Flo 200 and 0.03% Triton X-100. Finally, the slides were mounted with anti-fade medium (01100079, Biosharp) and imaged using a Leica SP8 confocal microscope (TCS SP8 DLS, Leica).

Whole-mount in situ hybridization

Zebrafish embryos from one-cell stage to 72 hpf were collected and fixed in 4% ribonuclease (RNase)-free PFA at 4°C for ≥24 h. The embryos were washed three times in PBS and manually dechorionated. They were dehydrated in a graded methanol series (25%, 50%, 75%, 100% in PBS, 15 min each) and stored in 100% methanol at −20°C for ≥2 h. Embryos were rehydrated in a reverse methanol gradient (5 min each) and washed in PBST. Embryos older than 24 hpf were treated with proteinase K (10 μg/mL in PBST) for 8–30 min depending on age, post-fixed in 4% PFA for 20 min, and washed five times with PBST for 5 min each. Pre-hybridization was performed in hybridization mix (50% formamide, 5× saline-sodium citrate (SSC), 0.1% Tween-20, 50 μg/mL heparin, 500 μg/mL transfer RNA (tRNA), pH 6.0) at 65°C for 2 h. Hybridization was carried out overnight at 65°C in fresh hybridization mix containing 1:500 RNase inhibitor and digoxigenin-labeled riboprobes (30–100 ng per 200 μL). After hybridization, embryos were washed sequentially at 65°C in hybridization mix (without heparin/tRNA), hybridization mix/SSC mixtures, 2× SSC, and 0.2× SSC, and then gradually transitioned to PBST at room temperature. Blocking was performed in PBST with 2 mg/mL BSA and 2% normal goat serum for 3–4 h at room temperature. Embryos were incubated with anti-digoxigenin-AP Fab fragments (1:5000) at 4°C overnight with gentle shaking. Following antibody incubation, embryos were washed extensively in PBST, equilibrated in alkaline phosphatase buffer (100 mM Tris–HCl pH 9.5, 50 mM $MgCl_2$, 100 mM NaCl, 0.1% Tween-20), and developed in the dark with nitro blue tetrazolium (NBT)/5-bromo-4-chloro-3-indolyl phosphate (BCIP) substrate. Color development was monitored every 15 min and stopped with PBST washes before imaging.

Hybridization chain reaction-RNA-FISH

Hybridization chain reaction (HCR)-RNA-fluorescence in situ hybridization (FISH) was performed on HEK293T cells and zebrafish testis sections as previously described [28]. A set of 24 pairs of split-initiator probes for zebrafish *THOR* was designed (Supplementary Table S1). Briefly, the fixed HEK293T cells or zebrafish testis sections were washed twice for 5 min each in PBS, and then incubated in 70% ethanol for 1 h for permeabilization. Primary hybridization was performed in hybridization buffer [30% formamide, 5× SSC, 9 mM citric acid (pH 6.0), 0.1% Tween 20, 50 μg/mL heparin, 1× Denhardt's solution, 10% dextran sulfate] containing pooled split-initiator probes (final concentration 4 nM) for 12–16 h at 37°C. Following hybridization, slides were washed four times for 5 min each with probe wash buffer [30% formamide, 5× SSC, 9 mM citric acid (pH 6.0), 0.1% Tween 20, 50 μg/mL heparin, 1× Denhardt's solution, 10% dextran sulfate] at 37°C, and then twice for 5 min each with 5× saline-sodium citrate with Tween 20 (SSCT) at room temperature. Hairpin probes H1 and H2 were separately denatured at 95°C for 90 s and cooled down to room temperature for 30 min to form hairpins. Slides were incubated with amplification buffer (5× SSC, 0.1% Tween 20, 10% dextran sulfate) containing hairpin probes (final concentration 60 nM) for 12–16 h in the dark at room temperature. Slides were washed five times for 5 min each with 5× SSCT at room temperature. Nuclei were stained with DAPI (1:5000 in PBS) for 5 min at room temperature. Coverslips were mounted with anti-fade mounting medium and stored in the dark at 4°C until imaging with a fluorescence microscope. Spermatocytes were identified by their larger nuclei and lower levels of chromatin condensation (indicated by dimmer DAPI fluorescence signals) on zebrafish testis sections.

RNA sequencing

Total RNA samples of WT and *THOR*$^{-/-}$ zebrafish testes (6 mpf) were sent to Icongene Biotech (Wuhan, China) for RNA sequencing. High-quality RNA samples (RNA integrity number (RIN) $\geq$8.0) were selected for library preparation using the NEBNext Ultra II RNA Library Prep Kit (E7770S, NEB) according to the manufacturer's instructions. Paired-end sequencing (150 bp) was performed on the Illumina NovaSeq 6000 platform. For each cDNA library, 6 G base raw reads were generated. RNA-seq data were analyzed as previously described [29, 30]. Briefly, raw reads in fastq format were first processed with fastp (v0.12.4) using the default parameters to remove low-quality reads. STAR (v2.7.5c) software was used to align the clean reads to the zebrafish reference genome (Danio_rerio.GRCz11.dna.primary_assembly.fa). Read counts for genes and transcripts were generated using featureCounts (v2.0.1). Differentially expressed genes (DEGs) were identified by DESeq2 (v1.22.1) using the thresholds of adjusted *P*-value $\leq$0.05 and |log2FC| $\geq$ 1. Gene Ontology (GO) and Kyoto Encyclopedia of Genes and Genomes (KEGG) enrichment analyses were performed by ClusterProfiler (v3.12.032).

RNA pulldown and LC–MS/MS (liquid chromatography-tandem mass spectrometry) assay

The RNA pulldown assay was performed using the F2-RNA pulldown kit (FI8701, Fitgene, Guangzhou, China) according to the manufacturer's instructions. Briefly, F2-tagged *THOR* sense and antisense probes were synthesized by in vitro transcription. The primers used for F2-tagged probe production are provided in Supplementary Table S1. Zebrafish testes from about 100 adult males were collected and homogenized in lysis buffer supplemented with protease inhibitor (1%) and RNase inhibitor (0.5%). The samples were sonicated on ice until the solution became mostly clear, followed by centrifugation at 12 000 × g for 15 min at 4°C. The supernatant was transferred to a new RNase-free tube. A 30 μL aliquot was collected as the input, and the remainder was reserved for the RNA pulldown assay. The F2-tagged probes were denatured at 95°C for 3 min, immediately placed on ice for 1 min, and then mixed with 50 μL of RNA structure buffer and 1 μL of RNase inhibitor, followed by incubation at room temperature for 30 min. Probes were then incubated with ligand-conjugated magnetic beads on a mixer at room temperature for 30 min. After two washes, the zebrafish testis protein sample was added, and the mixture was incubated at 4°C for 2–4 h. The magnetic beads were rinsed for three times. The bound proteins were eluted by adding 50 μL of elution buffer to the magnetic beads, followed by vortexing for 20 s and incubating on a mixer at room temperature for 10–15 min. The supernatant was collected and stored at −80°C. The bound proteins were identified by LC–MS/MS (Analysis and Testing Center, Institute of Hydrobiology, Chinese Academy of Sciences). Candidate *THOR*-interacting proteins were screened from the LC–MS/MS results of *THOR*-sense (S) and *THOR*-antisense (A) groups based on two criteria: (1) proteins exclusively detected in the *THOR*-sense group; (2) proteins detected in both groups, but significantly enriched in the *THOR*-sense group [proteins were considered enriched in the *THOR*-sense group if peptide-spectrum matches (PSMs) S-A $\geq$ 2 and S/A $\geq$ 1.5]. Proteins meeting either of the two criteria were defined as candidate *THOR*-interacting proteins.

Protein–protein interaction network analysis

Protein–protein interaction (PPI) network analysis was performed on candidate *THOR*-interacting proteins using the Search Tool for the Retrieval of Interacting Genes/Proteins (STRING) online database (version 11.5) (https://string-db.org/). All analyses were performed with default built-in parameters for zebrafish (*Danio rerio*) species background. No customized thresholds or modified settings were applied. The resulting interaction network was further visualized and modularly clustered within the STRING platform.

RNA immunoprecipitation assay

An RNA immunoprecipitation (RIP) assay was performed as previously described [31]. The zebrafish *THOR* and FLAG-tagged *sycp3* expression plasmids were co-transfected into HEK293T cells. After 48 h, cells were washed with PBS and lysed in the RIP lysis buffer (50 mM Tris–HCl pH 7.5, 150 mM NaCl, 1% NP-40, 0.5% sodium deoxycholate, 0.1% SDS) supplemented with 1 mM dithiothreitol (DTT), 100 U/mL RNasin Ribonuclease Inhibitor, and 1× protease inhibitor cocktail. For endogenous RIP assay, zebrafish testes from about 50 adult males were collected and homogenized in the RIP lysis buffer. Cell lysates were sonicated, followed by centrifugation at 12 000 × g for 15 min at 4°C. The supernatant was transferred to a new tube and stored on ice. A 50 μL aliquot was collected as input. For exogenous RIP assay, the supernatant was incubated with anti-FLAG magnetic beads at 4°C for 4 h with rotation. For endogenous

RIP assay, 10 μg of the anti-Sycp3 antibody (CZPA3, China Zebrafish Resource Center) was first added to the supernatant and incubated overnight at 4°C. Subsequently, protein A/G magnetic beads were added and incubated for 2 h at 4°C with rotation. Beads were washed five times with cold RIP wash buffer and once with PBS. Bound RNA-protein complexes were eluted in 100 μL TE buffer containing 0.5% SDS and 100 μg/mL Proteinase K at 55°C for 30 min. RNA was extracted from the eluate and the input sample using TRIzol LS Reagent (10296028CN, Thermo Fisher Scientific) according to the manufacturer's protocol. Precipitated Sycp3 protein was detected by Western blot. The levels of *THOR* were detected by reverse transcription and qPCR. The interaction strength between *THOR* and Sycp3 was evaluated by calculating 2^(-Ct[IP] − Ct[Input]). To confirm the specificity of RIP experiments, the normal IgG antibody and the mRNA fragment of *eef1a1l1* (a common housekeeping gene) were used as negative controls.

Cycloheximide chase assay

The zebrafish *THOR* and FLAG-tagged *sycp3* expression plasmids were co-transfected into HEK293T cells. After 36 h, cells were treated with cycloheximide (CHX) (C112766, Aladdin, Shanghai, China) at a final concentration of 100 μg/mL. Cells were harvested at 0, 1.5, 3, and 4.5 h after CHX treatment. Protein samples were prepared and stored at −20°C. Western blot was performed to detect the half-life of Sycp3 protein. Relative protein expression was quantified by normalization to alpha-tubulin.

Statistical analysis

GraphPad Prism 8 was used for data analysis and visualization. Immunofluorescence images were captured and quantitatively analyzed using Leica Application Suite X software. Statistical analysis was performed using the unpaired Student *t*-test. Results with error bars represented as mean ± SD. *P*-values less than 0.05 were considered significant. Statistical significance is indicated as follows: $*P < 0.05$, $**P < 0.01$, $***P < 0.001$, $****P < 0.0001$. Unless otherwise noted, all experiments were performed with at least three independent replicates.

Results

THOR is specifically enriched in the differentiating germ cells of zebrafish testis

The genomic location of zebrafish *THOR* has not yet been determined in the Zebrafish Information Network (https://zfin.org/) database. We cloned and sequenced the zebrafish *THOR* cDNA fragment, and aligned its sequence to the zebrafish reference genome (GRCz11) in the Ensembl database. We found that the *THOR* sequence matched 100% to the region of Chr1: 7 835 710–7 837 877, which was flanked by *arglu1b*, *en1b*, *radil*, and *mmd2b* genes (Figure 1A). Moreover, we found that *THOR* is located within the intron 2 of another lncRNA gene annotated as *ENSDARG00000117359*, and its transcription direction is opposite to that of *ENSDARG00000117359* (Figure 1A). To validate the transcription orientation of *THOR*, we performed strand-specific reverse transcription by adding *THOR* positive-strand and negative-strand specific primers, respectively (Figure 1B). The resulting first-strand cDNAs were used as PCR templates, and electrophoresis results showed that *THOR* is transcribed unidirectionally as expected (Figure 1C).

We then examined the spatiotemporal expression pattern of *THOR* in zebrafish. Whole-mount in situ hybridization and qPCR assays revealed a ubiquitous yet low-level distribution of *THOR* from one-cell stage to 72 hpf (Supplementary Figure S1A and B). Reverse transcription-polymerase chain reaction (RT-PCR) and qPCR assays across 10 representative organs (brain, eye, gill, gut, heart, kidney, liver, muscle, spleen, and gonad) from adult male and female zebrafish (90 dpf) showed that *THOR* is predominantly expressed in the testis (Supplementary Figure S1C and D). HCR-RNA-FISH was performed on zebrafish testis sections and *THOR*-overexpressing cell lines, respectively, to determine the cell types and subcellular localization of *THOR*. Our results showed that *THOR* is predominantly expressed in spermatocytes (Figure 1D), which were featured by a larger nuclear size and a lower degree of chromatin condensation. At the subcellular level, *THOR* is localized in both the cytoplasm and the nucleus (Figure 1E). Finally, using publicly available single-cell RNA-seq datasets of human testis [32] and mouse testis [33], we analyzed the expression of *THOR* orthologs in humans (*ENSG00000226856*) and mice (*ENSMUSG00000101700*) across various testicular cell types (Figure 1F–I). The human and mouse *THOR* orthologs were enriched in male germ cells (spermatogonia, spermatocytes, and spermatids), which was consistent with our results observed in zebrafish.

Knockout of *THOR* impairs spermatogenesis process in zebrafish

To investigate the physiological functions and regulatory mechanisms of *THOR* in zebrafish testis, we utilized CRISPR-Cas9 technology to construct a *THOR*-deleted zebrafish model by co-injecting two highly efficient sgRNAs spanning the conserved region of *THOR* (Figure 2A). Genetically stable *THOR* homozygotes ($THOR^{-/-}$) were screened and propagated. No gross morphological defects or decreased hatching rates were observed in the $THOR^{-/-}$ zebrafish. PCR and Sanger sequencing of the *THOR* genomic fragment confirmed a 1846 bp deletion in $THOR^{-/-}$ zebrafish (Figure 2A and B). Moreover, a qPCR assay showed a complete depletion of *THOR* transcript in $THOR^{-/-}$ testes at 90 dpf (Figure 2C). These results confirmed the successful construction of a *THOR* knockout zebrafish model.

Next, we examined the testis development status of $THOR^{-/-}$ zebrafish at different stages (90, 180, and 270 dpf). In terms of testis morphology, no significant differences were observed between WT and $THOR^{-/-}$ zebrafish (Supplementary Figure S2). Histological analysis revealed varying degrees of vacuolation in the region representing mature spermatozoa on the testis sections of $THOR^{-/-}$ zebrafish (Figure 2D–F). Notably, at 180 dpf, the proportion of mature spermatozoa regions in the $THOR^{-/-}$ group was markedly reduced to 34%, compared to 64% in the WT group (Figure 2G–I). To distinguish spermatocytes at different meiotic stages, we performed immunofluorescence staining using the synaptonemal complex protein 3 (Sycp3) antibody [26] in WT and $THOR^{-/-}$ testis sections (Figure 3A–F). At 180 dpf, we observed a significant decline in the proportion of leptotene (L) cells, accompanied by an increase in the

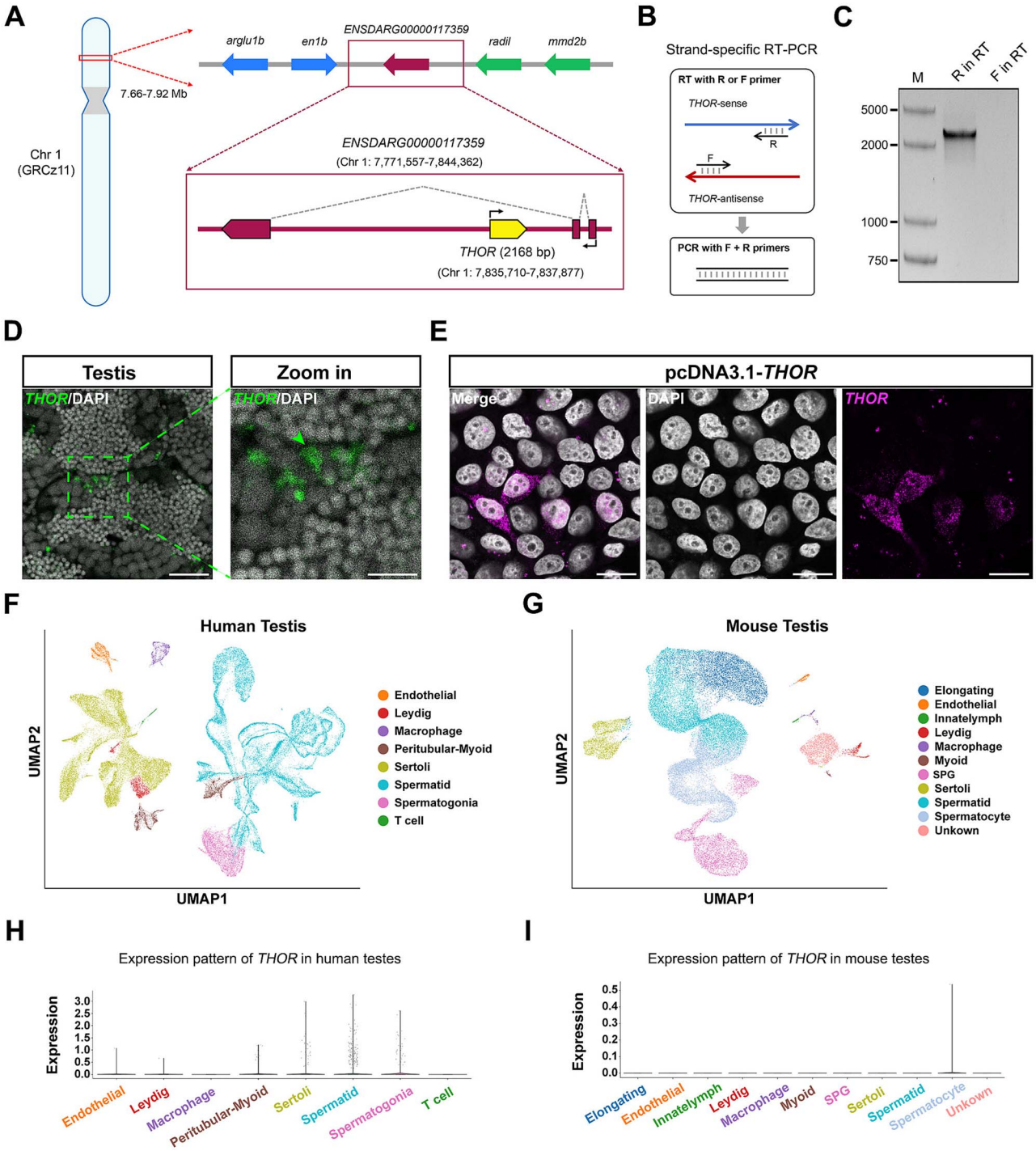


Figure 1. Identification of the genomic location and expression patterns of zebrafish *THOR*. (A) The genomic location of zebrafish *THOR* determined by sequencing and aligning its cDNA to the reference genome (GRCz11). (B) Schematic diagram of the strand-specific RT-PCR assay to determine the transcriptional orientation of *THOR*. (C) Gel image of strand-specific RT-PCR confirming the exclusive presence of the *THOR* sense strand in zebrafish testes. (D) HCR-RNA-FISH showing the expression distribution of *THOR* on zebrafish testis sections at 180 dpf. The arrowhead indicates spermatocytes, featured by larger nuclear size and lower degree of chromatin condensation. Scale bars, 50 μm (left panel) and 20 μm (right panel). (E) Subcellular localization of ectopically expressed zebrafish *THOR* in HEK293T cells revealed by HCR-RNA-FISH. Scale bars, 50 μm. (F and G) Uniform Manifold Approximation and Projection (UMAP) plots showing the cell types of human (F) and mouse (G) testes identified by scRNA-seq. (H and I) Violin plots showing the expression patterns of human (H) and mouse (I) *THOR* orthologs across distinct cell types identified by scRNA-seq.

proportion of early zygotene (EZ) cells (Figure 3B and E). According to published literature [34, 35], we selected a series of marker genes for male germ cells from spermatogonia to spermatozoa, and analyzed their expression via qPCR. We found that most marker genes, including *vasa* (*DEAD (Asp-Glu-Ala-Asp) box polypeptide 4*), *sycp3*, *ARL6 interacting reticulophagy regulator 1* (*arl6ip1*), *cyclin B3* (*ccnb3*), *cilia and flagella associated protein 52* (*cfap52*), and *sperm associated antigen 8* (*spag8*), were downregulated in $THOR^{-/-}$ testes (Figure 3G). These results suggest

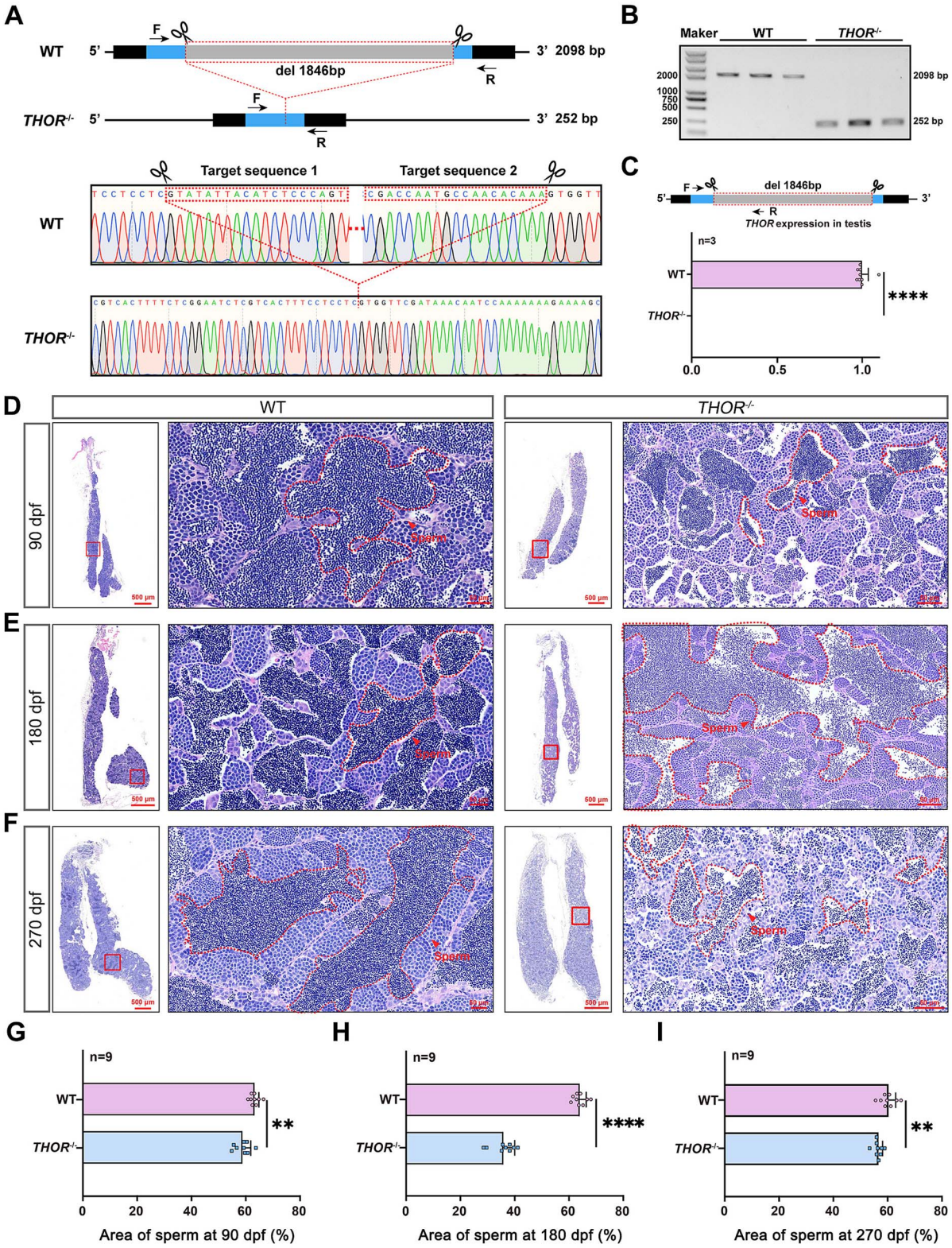


Figure 2. Knockout of *THOR* causes testicular morphological defects in zebrafish. (A) Generation of *THOR* knockout zebrafish model by co-injecting Cas9 protein with two sgRNAs spanning the conserved region of *THOR* into zebrafish embryos. Sanger sequencing confirmed a 1846 bp deletion in the *THOR* genomic locus. (B) Genotyping of WT and *THOR* knockout homozygotes by PCR and agarose gel electrophoresis. (C) qPCR validation of *THOR* knockout at the mRNA level using WT and $THOR^{-/-}$ testes at 90 dpf. Data are presented as mean ± SD ($n = 3$). $^{***}P < 0.001$. (D–F) Histological analysis of WT and $THOR^{-/-}$ testes at 90 dpf (D), 180 dpf (E), and 270 dpf (F). The corresponding panoramic images of zebrafish testis sections are shown in the left panels. Regions representing mature sperm are indicated by dashed lines. Scale bars, 50 μm. (G–I) Quantitative analysis of the dashed areas suggests impaired spermatogenesis in $THOR^{-/-}$ testes at 90 dpf (G), 180 dpf (H), and 270 dpf (I). Data are presented as mean ± SD ($n = 3$). $^{*}P < 0.05$, $^{**}P < 0.01$.

that spermatogenesis may be impaired in $THOR^{-/-}$ zebrafish.

Reduced sperm count, decreased sperm motility, abnormal sperm ultrastructure, and declined fertilization rates in *THOR* $^{-/-}$ zebrafish

To examine the effect of *THOR* knockout on the reproductive capacity of male zebrafish, we performed sperm counting on the collected semen from WT and $THOR^{-/-}$ zebrafish at 180 dpf. Compared with WT controls, the sperm concentration in $THOR^{-/-}$ zebrafish decreased by 38.7% (1.5×10^7 per mL to 9.2×10^6 per mL) (Figure 4A and B). CASA showed that although the proportions of motile and progressive sperm were not significantly different (Figure 4C), motility parameters, including straight-line velocity (VSL), curvilinear velocity (VCL), and average path velocity (VAP), for motile and progressive sperm were decreased in $THOR^{-/-}$ zebrafish (Figure 4D and E). The VSL, VCL, and VAP of motile sperm decreased by 22.51%, 17.3%, and 15.76%, respectively (Figure 4D). Meanwhile, the VSL, VCL, and VAP of progressive sperm decreased by 9.6%, 15.02%, and 10.9%, respectively (Figure 4E). Moreover, sperm ultrastructure of WT and $THOR^{-/-}$ zebrafish were observed by scanning electron microscopy (Figure 4F). Morphometric analysis revealed that $THOR^{-/-}$ sperm exhibited shorter flagella (30.80 ± 1.87 μm vs 32.56 ± 2.05 μm) and enlarged heads, manifested as increased head width and head length (Figure 4G).

Finally, we analyzed the fertilization rate of $THOR^{-/-}$ zebrafish through mating experiments (Figure 4H). The WT♀ × WT♂ group showed a high fertilization rate ($94.66 \pm 2.73\%$). The fertilization rate of WT♀ × $THOR^{-/-}$♂ group decreased to $50.89 \pm 7.09\%$, while the $THOR^{-/-}$♀ × WT♂ group still had an approximately 80% fertilization rate (Figure 4I), suggesting that $THOR^{-/-}$ male zebrafish are the primary contributors to the decreased fecundity. Meanwhile, the sex ratio of WT and $THOR^{-/-}$ zebrafish was quantified at 90 dpf. No statistically significant differences were observed (Figure 4J).

Transcriptome analysis revealed dysregulated expression of cell cycle-related genes in *THOR* $^{-/-}$ zebrafish testes

To elucidate the molecular mechanisms underlying the impaired spermatogenesis in $THOR^{-/-}$ zebrafish, we performed RNA-seq analysis on WT and $THOR^{-/-}$ testes at 180 dpf. Quality control data, including total reads, total mapping rates, and unique mapping rate, are shown in Supplementary Figure S3A and Supplementary Table S2. Correlation heatmap and principal component analysis showed that our RNA-seq samples exhibited good intra-group correlation ($R^2 \geq 0.93$) and distinct inter-group differences (Figure 5A and Supplementary Figure S3B). A total of 2237 DEGs were identified, including 995 downregulated and 1242 upregulated genes (Figure 5B, Supplementary Figure S3C, and Supplementary Table S3). GO enrichment analysis showed that GO terms related to cell cycle and cell death were significantly enriched in DEGs (Figure 5C and Supplementary Table S4). Gene set enrichment analysis also showed that genes in the "Regulation of mitotic cell cycle" gene set were markedly downregulated in $THOR^{-/-}$ testes (Figure 5D).

To better illustrate the expression patterns of cell cycle-related DEGs, we generated an expression heatmap for these genes based on our RNA-seq data (Figure 5E). We found that *cyclin-dependent kinase inhibitor 1D* (*cdkn1d*), *forkhead box O1 a* (*foxo1a*), *TSC complex subunit 1a* (*tsc1a*), *TSC complex subunit 2* (*tsc2*), and *transforming growth factor, beta 2* (*tgfb2*) were upregulated in $THOR^{-/-}$ testes, while *atrx* (*ATRX chromatin remodeler*) and *rad21b* (*RAD21 cohesin complex component b*) were downregulated. The expression changes of these cell cycle-related genes were further validated by qPCR (Figure 5F). Interestingly, we noticed that the majority of downregulated genes belonged to the *pimr* (Pim proto-oncogene, serine/threonine kinase, related) family, suggesting that there may be a specific regulatory relationship between *THOR* and *pimr* family genes.

To further validate whether *THOR* is involved in the regulation of mitosis, we performed pH3 (phosphorylated histone H3) immunostaining to detect mitotically active cells on WT and $THOR^{-/-}$ testis sections at 90, 180, and 270 dpf, respectively. Immunofluorescence images and quantitative results revealed a certain degree of reduction in the number of pH-3-positive cells in $THOR^{-/-}$ testes at 180 dpf (Supplementary Figure S4), suggesting that *THOR* deficiency may impair mitotic progression in zebrafish testes.

Identification of *THOR*-interacting proteins in zebrafish testes through RNA pulldown assay

Long non-coding RNAs can exert functions through diverse mechanisms, including interacting with proteins, chromatin, or other RNA molecules. To identify *THOR*-interacting proteins in zebrafish testes, we performed RNA pulldown assay by incubating F2-tagged sense and antisense *THOR* probes with zebrafish testis lysates, respectively (Figure 6A and B). LC–MS/MS analysis was employed to detect RNA pulldown-precipitated proteins (Figure 6C). We identified 601 proteins in the *THOR*-sense group and 286 proteins in the *THOR*-antisense group. Candidate *THOR*-interacting proteins included 337 proteins exclusively detected in the *THOR*-sense group and another 149 proteins enriched in the *THOR*-sense group (enrichment threshold: PSMs S-A $\geq$2 and PSMs S/A $\geq$1.5) (Figure 6D and Supplementary Table S5).

Function annotation of these potential *THOR*-interacting proteins was performed (Supplementary Table S6). GO enrichment analysis revealed significant enrichment of the terms "RNA splicing," "Ribonucleoprotein complex biogenesis," "mRNA processing," "Structural constituent of ribosome," and "mRNA binding" (Figure 6E and Supplementary Figure S5A and B). KEGG enrichment analysis showed that the terms "Ribosome" and "Spliceosome" were significantly enriched (Figure 6F). PPI network analysis identified four core functional modules: (i) ribosome biogenesis and translation, (ii) RNA splicing and processing, (iii) chromatin architecture, and (iv) meiotic progression (Figure 6G and H and Supplementary Figure S5C and D). Based on the functional analysis of potential *THOR*-interacting proteins, we speculate that *THOR* may play important roles in translation, pre-mRNA splicing, chromatin structure, and meiosis progression in zebrafish testes.

THOR interacts with Sycp3 and stabilizes its protein level in zebrafish testes

Notably, three core components of the synaptonemal complex, Sycp1, Sycp2, and Sycp3, were identified among the candidate *THOR*-interacting proteins (Supplementary Table S5). Sycp3 was ranked 209th (PSMs = 2, Sum Peptide Score = 3.044)

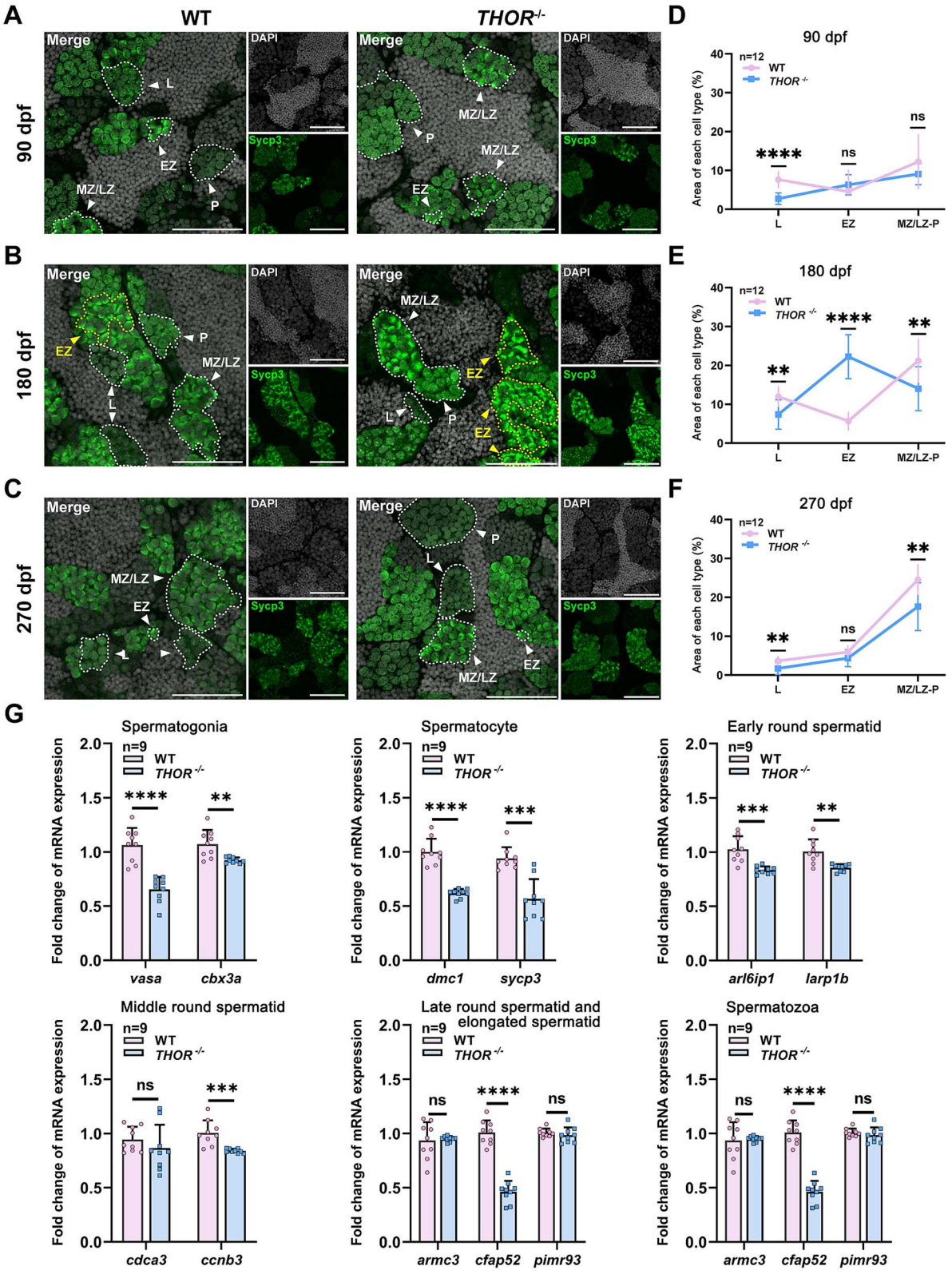


Figure 3. Impaired spermatogenesis process in *THOR*$^{-/-}$ zebrafish testes. (A–C) Immunofluorescence staining of the meiotic marker Sycp3 on testicular sections of WT and *THOR*$^{-/-}$ zebrafish at 90 dpf (A), 180 dpf (B), and 270 dpf (C). The areas related to different types of spermatogenic cells (L, EZ, MZ/LZ, P) are marked by dashed lines. Scale bars, 50 μm. Representative cell morphology images were taken with variable imaging parameters and uniformly adjusted for brightness/contrast to resolve diverse cell subtypes. Quantitative fluorescence intensity was quantified on raw images captured with identical acquisition settings. (D–F) Quantitative analysis of the areas of different types of Sycp3-positive spermatogenic cells at 90 dpf (D), 180 dpf (E), and 270 dpf (F). Data are presented as mean ± SD ($n = 12$). $^{*}P < 0.05$, $^{**}P < 0.01$, $^{****}P < 0.0001$. (G) Expression of marker genes at different stages of spermatogenesis in WT and *THOR*$^{-/-}$ testes at 180 dpf as detected by qPCR. Data are presented as mean ± SD ($n = 9$). $^{*}P < 0.05$, $^{**}P < 0.01$, $^{***}P < 0.001$, $^{****}P < 0.0001$.

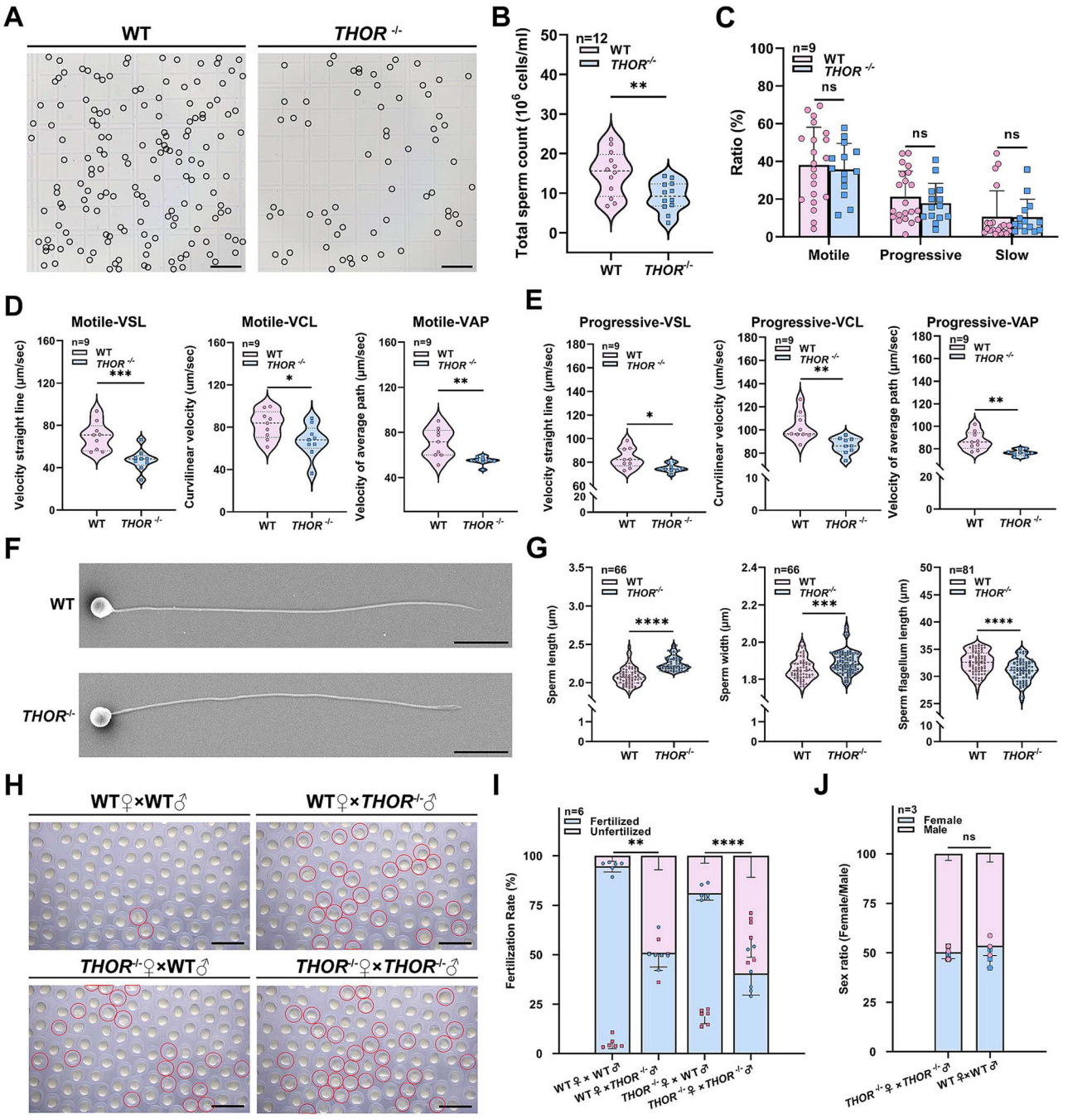


Figure 4. Loss of *THOR* results in reduced sperm count, decreased sperm motility, abnormal sperm ultrastructure, and declined fertilization rates. (A) Sperm count analysis of WT and $THOR^{-/-}$ zebrafish at 180 dpf. Scale bars, 50 μm. (B) $THOR^{-/-}$ zebrafish exhibited a significant decrease in sperm count at 180 dpf. Data are presented as mean ± SD ($n = 12$). (C) Proportions of different types of sperm (motile, progressive, and slow) in WT and $THOR^{-/-}$ zebrafish analyzed by a CASA system. (D, E) Velocity of motile (D) and progressive (E) sperm of WT and $THOR^{-/-}$ zebrafish. VSL, straight-line velocity. VCL, curvilinear velocity. VAP, average path velocity. $^{*}P < 0.05$, $^{**}P < 0.01$, $^{***}P < 0.001$, $^{****}P < 0.0001$. (F) The ultrastructure of sperm from WT and $THOR^{-/-}$ zebrafish at 180 dpf. Scale bars, 5 μm. (G) Quantitative morphometric analysis of the sperm head and flagellum. Data are presented as mean ± SD. (H) Mating experiments with different combinations of WT and $THOR^{-/-}$ zebrafish. Microscopic observation of the fertilized and unfertilized (marked by cycles) zebrafish embryos. Scale bars, 2000 μm. (I) Quantitative analysis of fertilization rates for embryos from different zebrafish mating combinations. Data are presented as mean ± SD ($n = 6$). $^{**}P < 0.01$; $^{****}P < 0.0001$. (J) Offspring sex ratio from WT and $THOR^{-/-}$ homozygous mating pairs. Data are presented as mean ± SD ($n = 3$).

among the 337 proteins exclusively detected in the *THOR*-sense group. Sycp1 (PSMs in the *THOR*-sense group = 21, PSMs S-A = 17, PSMs S/A = 5.25) and Sycp2 (PSMs in the *THOR*-sense group = 14, PSMs S-A = 8, PSMs S/A = 2.33) were ranked 18th and 88th among the 149 proteins enriched in the *THOR*-sense group, respectively. The synaptonemal complex is essential for homologous chromosome pairing, synapsis, recombination, and segregation during meiosis, and therefore its proper assembly and function are crucial for successful spermatogenesis [36, 37]. Particularly, we

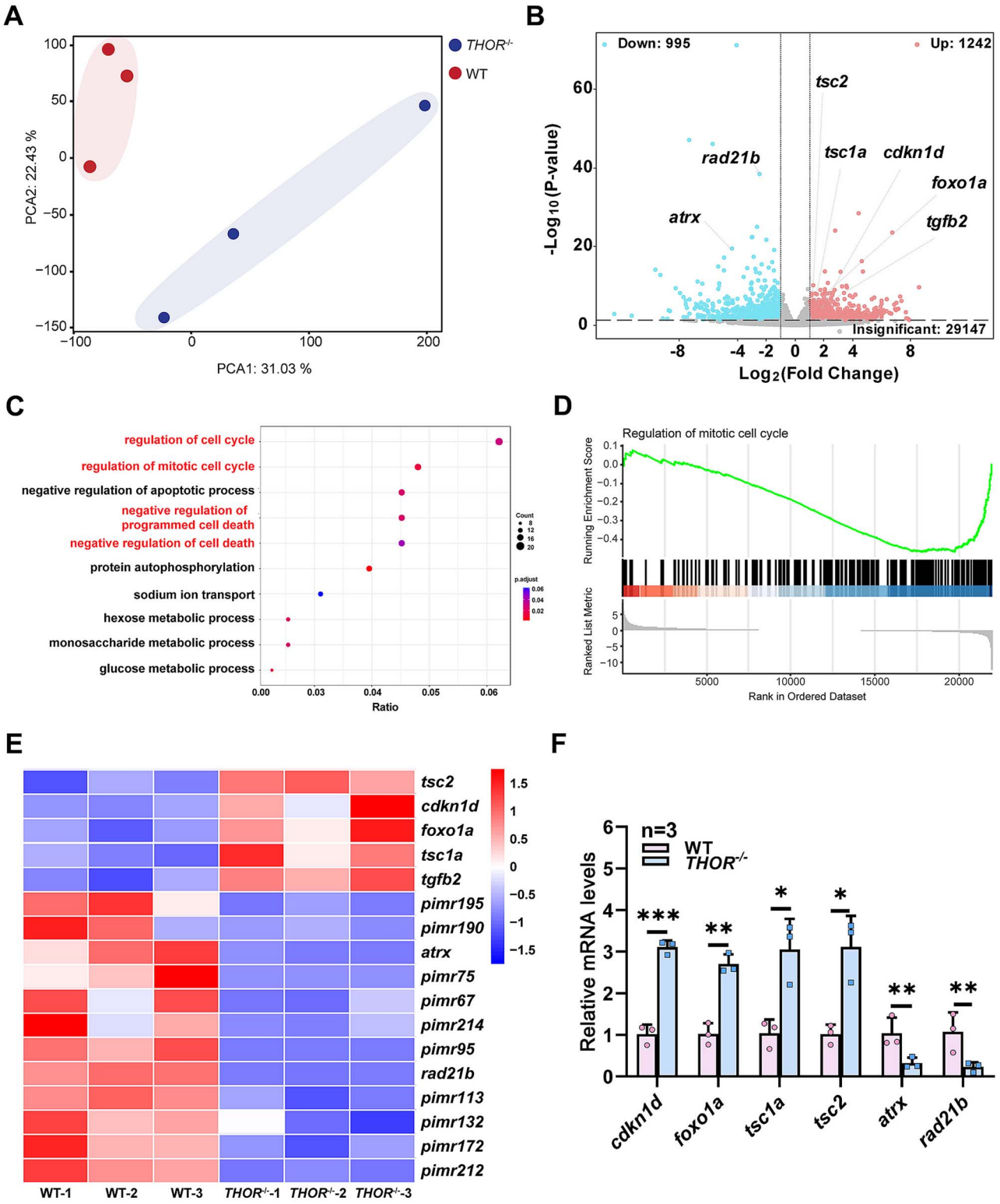


Figure 5. Transcriptome analysis revealed dysregulated expression of cell cycle-related genes in *THOR*$^{-/-}$ zebrafish testes. (A) Principal component analysis (PCA) revealed the overall difference in the testis transcriptome between WT and *THOR*$^{-/-}$ zebrafish testes at 180 dpf. (B) Volcano plot showing the DEGs between WT and *THOR*$^{-/-}$ testes. (C) GO enrichment analysis of DEGs showed that cell cycle-related genes were significantly enriched. (D) Gene set enrichment analysis plot showed that the gene set of "Regulation of mitotic cell cycle" was significantly downregulated in *THOR*$^{-/-}$ zebrafish testes. (E) Heatmap showing the expression pattern of DEGs related to regulation of mitotic cell cycle in WT and *THOR*$^{-/-}$ testes. (F) Validating the expression changes of cell cycle-related DEGs in *THOR*$^{-/-}$ testes by qPCR.

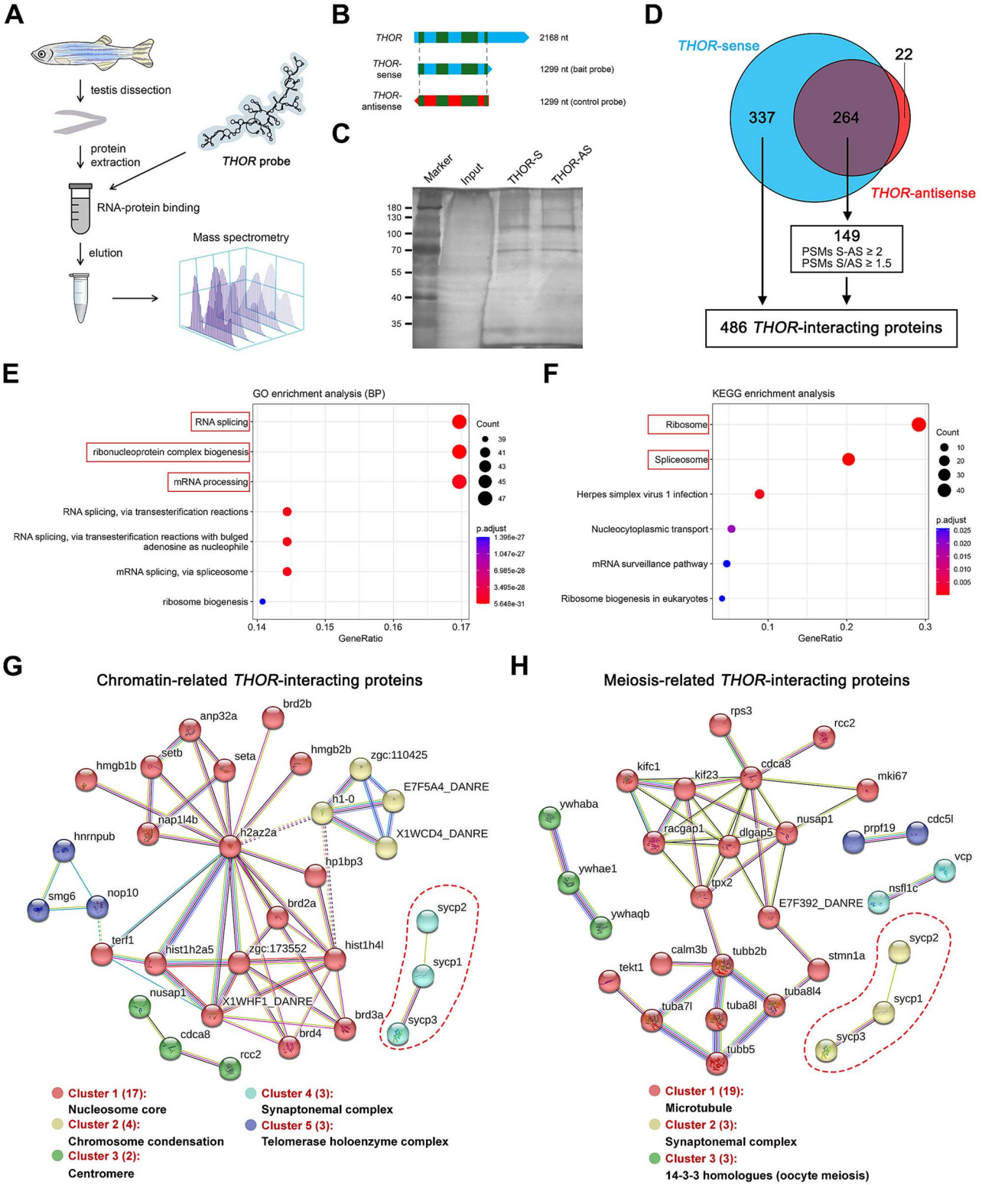


Figure 6. Identification and functional annotation of *THOR*-interacting proteins in zebrafish testes. (A) Experimental workflow for identifying *THOR*-interacting proteins in zebrafish testes. (B) Construction of the F2-tagged *THOR* sense and antisense probes used for RNA pulldown assay. (C) SDS-PAGE and silver staining of the *THOR*-interacting proteins from RNA pulldown assay. (D) Screening for potential *THOR*-interacting proteins by combining proteins unique to the *THOR*-sense group (337) and proteins enriched in the *THOR*-sense group (149). (E) GO enrichment analysis (Biological Process, BP) of the potential *THOR*-interacting proteins. (F) KEGG enrichment analysis of the potential *THOR*-interacting proteins. PPI networks of *THOR*-interacting proteins related to chromatin (G) and meiosis (H) are shown. The synaptonemal complex components Sycp1, Sycp2, and Sycp3 are marked with dashed lines.

indeed observed abnormalities in spermatocyte meiosis in *THOR*$^{-/-}$ zebrafish, leading us to hypothesize that *THOR* regulates meiosis progression through direct interaction with the synaptonemal complex.

To validate this hypothesis, exogenous and endogenous RIP assays were performed to confirm the direct interaction between *THOR* and Sycp3 (Figure 7A). RT-PCR and qPCR results of our in vitro RIP assay showed a strong interaction between *THOR* and Sycp3, as reflected by an 8.4-fold enrichment of *THOR* in the FLAG-Sycp3 IP group (Figure 7B and C). Consistent with exogenous RIP results, the endogenous *THOR* RNA fragment was also significantly enriched in the Sycp3 IP group (Figure 7D and E). Furthermore, we examined the protein levels of Sycp3 in WT and *THOR*$^{-/-}$ testes at 180 dpf by Western blot assay. Interestingly, protein levels of Sycp3, rather than Sycp1, were markedly reduced in *THOR*$^{-/-}$ testes (Figure 7F and G). We then assessed the effect of *THOR* overexpression on Sycp3 protein stability in HEK293T cells. We found that overexpression of *THOR* significantly increased the protein levels of heterologously expressed zebrafish Sycp3 in a dose-dependent manner, without affecting the *sycp3* mRNA levels (Figure 7G–I). To investigate whether *THOR* overexpression increases the half-life of Sycp3 protein, we performed a CHX chase assay in HEK293T cells. Our results showed that the degradation rate of Sycp3 protein was significantly reduced in the *THOR*-overexpressing cells (Figure 7K and L). These results suggest that *THOR* directly interacts with Sycp3 and stabilizes its protein level.

To further explore the physiological significance of the *THOR*-Sycp3 interaction in zebrafish testes, we examined the expression levels of Sycp3 protein in *THOR*$^{-/-}$ testes by immunofluorescence assay at 90, 180, and 270 dpf (Figure 8A). Quantitative results showed that the abundance of Sycp3 decreased to varying degrees in *THOR*$^{-/-}$ testes throughout all three stages (Figure 8B–D). Given the crucial role of Sycp3 in synaptonemal complex assembly, we performed dual immunostaining assays on chromosome spreads for Sycp1 and Sycp3 using WT and *THOR*$^{-/-}$ testes at 180 dpf. We found that in WT spermatocytes, Sycp3 exhibited complete co-localization with Sycp1 along the chromosomal axis with a continuous and intact synaptonemal complex structure (Figure 8E). Meanwhile, spermatocytes from *THOR*$^{-/-}$ testes exhibited a significantly higher frequency of fragmentation or discontinuity of Sycp3-labeled chromosome axes (Figure 8F). These results provide further evidence that *THOR* plays an important role in maintaining the meiotic progression of spermatocytes in zebrafish testes.

Discussion

In this study, we characterized the genomic locus and expression pattern of zebrafish *THOR*, confirming it as a conserved, testis-enriched lncRNA. Using a *THOR* knockout zebrafish model, we demonstrate that *THOR* plays an important role in spermatogenesis; its loss leads to defective spermatocyte meiosis and a marked reduction in sperm number. Mechanistically, RNA-seq analysis revealed that *THOR* knockout primarily dysregulates cell cycle-related genes. Furthermore, RNA pull-down and RIP assays identified Sycp3, a core component of the synaptonemal complex, as a direct interacting partner of *THOR* in the zebrafish testis. We find that *THOR* maintains Sycp3 protein levels, thereby preserving the structural integrity of the synaptonemal complex and supporting normal meiotic progression. To our knowledge, this is the first report of an lncRNA interacting with the synaptonemal complex to regulate meiosis. These findings expand our understanding of how lncRNAs control spermatogenesis and contribute to male infertility.

Based on our analysis, zebrafish *THOR* is located within an ultra-long intron (~70 kb) of the lncRNA gene *ENSDARG00000117359*, situated 6.5 kb from exon 2 and 63.5 kb from exon 3 of *ENSDARG00000117359*. Given the substantial distance between *THOR* and its host or neighboring genes, it is unlikely that *THOR* knockout would affect the expression of these genes, consequently causing off-target effects. Additionally, based on our RNA-seq data, no significant differences in the expression levels of several *THOR* neighboring genes were observed between WT and *THOR*$^{-/-}$ testes, further ruling out the possibility that *THOR* deletion could affect neighboring transcripts.

The sequence conservation and testis-enriched expression pattern of lncRNA *THOR* have been reported in humans, mice, and zebrafish [14, 23]. Although the vast majority of current research on *THOR* has focused on its role in tumors [14–20, 38–40], its physiological function in normal testicular tissue also warrants attention. A previous study has shown that knockout of *THOR* reduces zebrafish fertilization rates [14]; however, the pathological alterations at the tissue, cellular, and molecular levels remain to be elucidated. In this study, we established a comprehensive phenotypic profile of the *THOR*-knockout zebrafish testis, by performing histological analysis and immunofluorescence and qPCR assays of testicular marker genes across different stages, along with sperm motility and ultrastructural analyses. These experimental data unequivocally demonstrate that *THOR* knockout impairs spermatogenesis and diminishes both sperm number and motility, thereby causing a decline in male reproductive capacity. Interestingly, by comparing the phenotype of our *THOR*-knockout zebrafish with that of mice [23], we observed both conserved and divergent roles of *THOR* between the two species. In addition to reduced sperm motility and fertility, *THOR*-knockout mice also exhibited smaller testicular size, reduced body size, and significantly decreased survival rates [23], which were not observed in our *THOR*-knockout zebrafish model. These findings suggest that the function of *THOR* in regulating spermatogenesis appears to be more tissue-specific in zebrafish.

An intriguing observation of this study is that the testicular phenotype of *THOR*$^{-/-}$ zebrafish is most prominent at 180 dpf, compared to 90 and 270 dpf. The exact reasons behind this phenomenon remain unclear. We speculate that this may be due to age-related differences in the requirement for *THOR* or Sycp3 in zebrafish testes. Under laboratory culture conditions, 90 dpf is generally considered the time when male zebrafish reach full sexual maturity. At 180 dpf, male zebrafish are at their peak reproductive capacity, and their testes exhibit continuous and vigorous spermatogenic activity. At 270 dpf, male zebrafish enter the early phase of testicular functional senescence, manifested as decreased mating efficiency and diminished sperm production. It's reasonable to speculate that the testis may be more sensitive to *THOR* deficiency at 180 dpf.

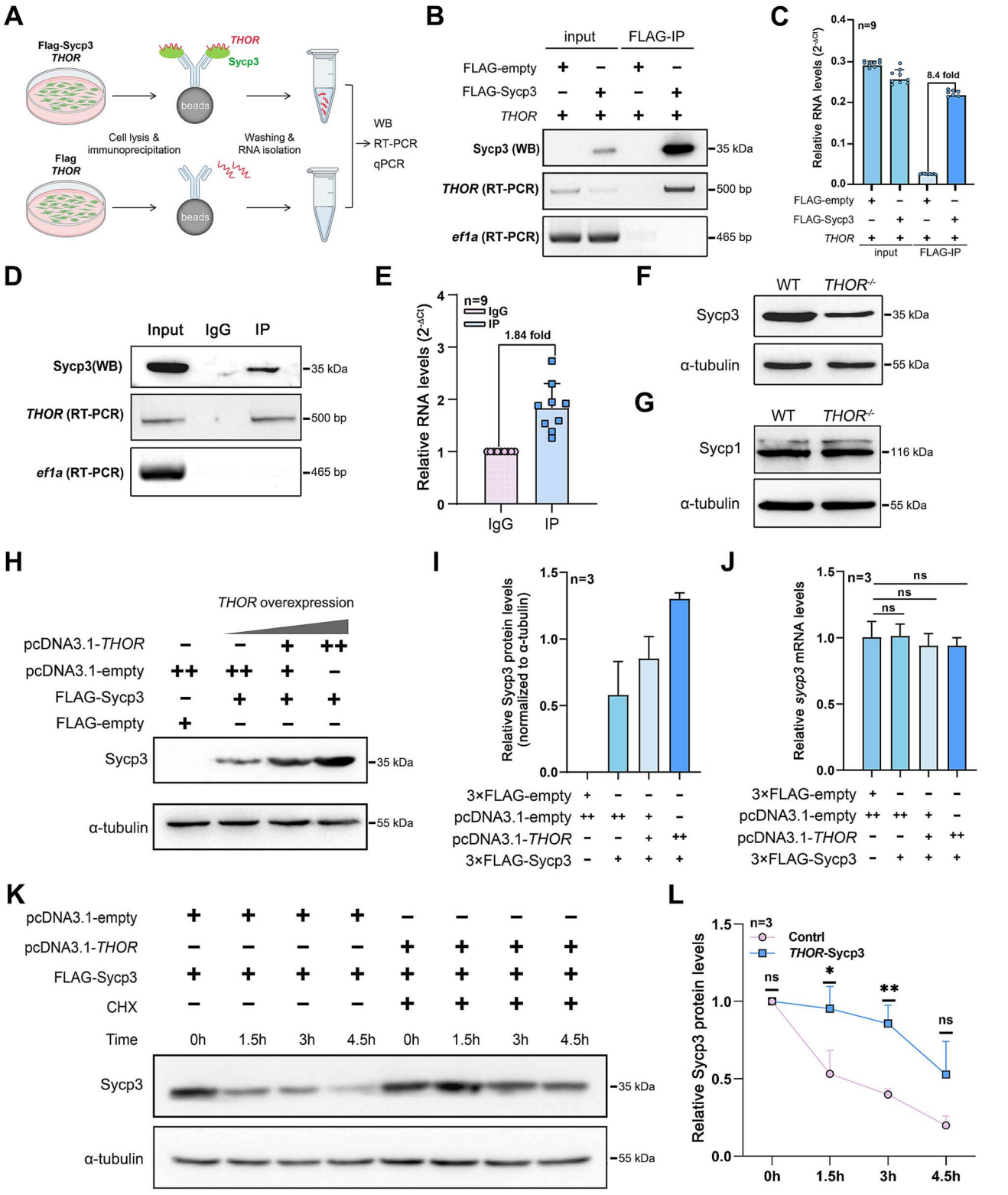


Figure 7. *THOR* directly interacts with Sycp3 and positively regulates its protein levels. (A) Technical workflow of RIP analysis validating the interaction between exogenously expressed *THOR* and Sycp3. (B) Western blot and RT-PCR results of the exogenous RIP assay. The mRNA fragment of *eef1a1l1*, a common housekeeping gene, was used as a negative control. (C) qPCR results of the exogenous RIP assay. *THOR* is enriched 8.4-fold in the FLAG-Sycp3 IP group. (D) Western blot and RT-PCR results of the endogenous RIP assay. The normal IgG antibody and the mRNA fragment of *eef1a1l1* were used as negative controls. (E) qPCR results of the endogenous RIP assay. *THOR* is enriched 1.84-fold in the Sycp3 IP group. (F and G) Detection of Sycp3 and Sycp1 protein levels in $THOR^{-/-}$ testes at 180 dpf by Western blot. (H) Western blot analysis showing increased Sycp3 protein levels upon *THOR* overexpression in a dose-dependent manner in HEK293T cells. (I) Quantitative analysis of the Sycp3 bands shown in (H). (J) qPCR analysis showing no significant alteration in *Sycp3* mRNA levels upon *THOR* overexpression. (K) CHX chase assay showing the half-life of Sycp3 protein in the control and *THOR* overexpression groups in HEK293T cells. (L) Quantitative analysis of the Western blot bands in CHX chase assay.

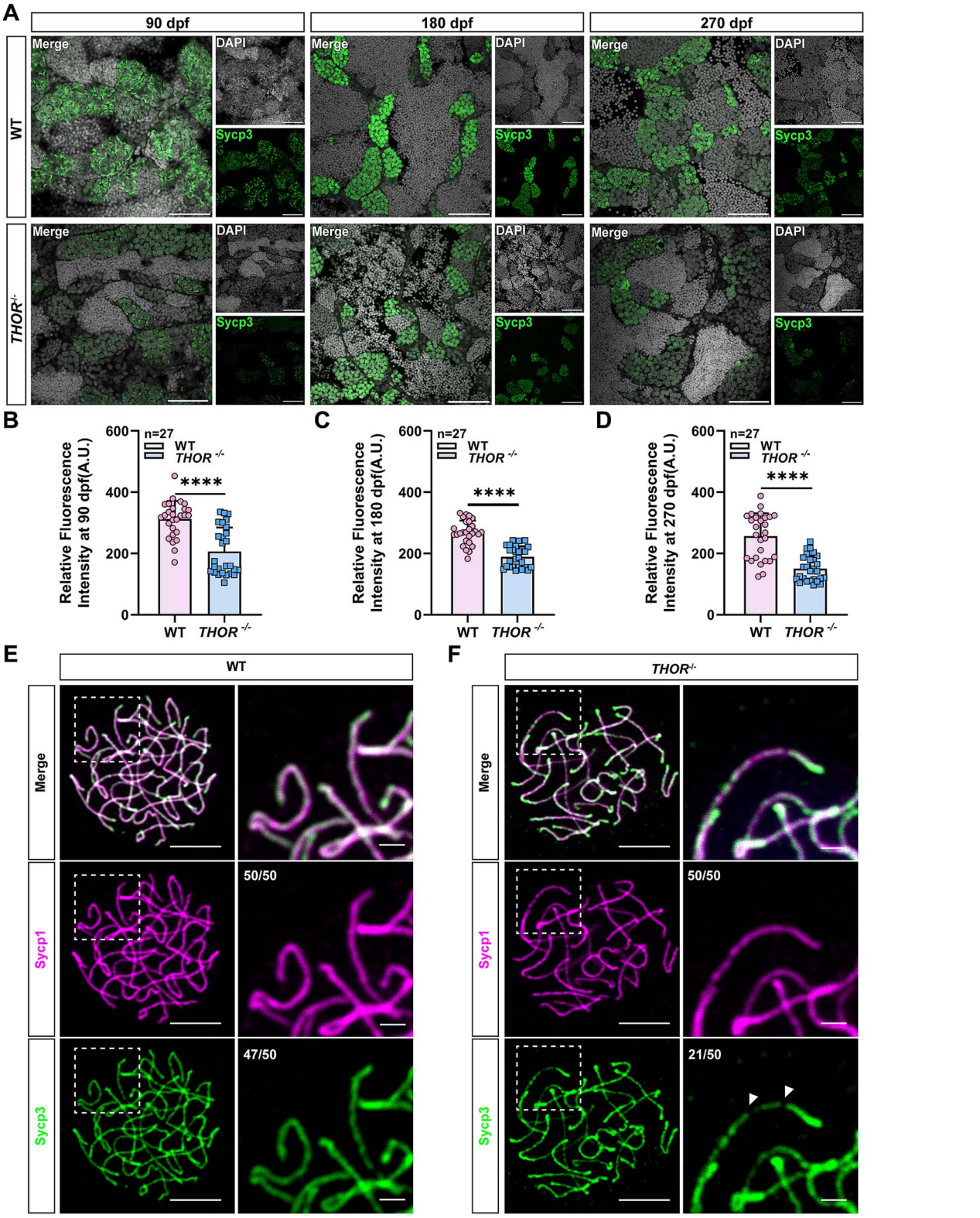


Figure 8. Loss of *THOR* reduces Sycp3 protein abundance and disrupts synaptonemal complex integrity in zebrafish spermatocytes. (A) Representative immunofluorescence images of Sycp3 in WT and $THOR^{-/-}$ testis sections at 90, 180, and 270 dpf. All tissue sections were imaged under identical microscope acquisition parameters. Scale bars, 50 μm. (B–D) Quantitative analysis of the relative Sycp3 fluorescence intensity at 90 dpf (B), 180 dpf (C), and 270 dpf (D). Data are presented as mean ± SD. **** $P < 0.0001$. (E and F) Dual immunostaining assays for Sycp1 (magenta) and Sycp3 (green) on chromosome spreads of WT (E) and $THOR^{-/-}$ (F) testes at 180 dpf. Arrowheads indicate the fragmented Sycp3 filaments in $THOR^{-/-}$ spermatocytes. Scale bars: 5 μm and 1 μm.

RNA-seq analysis has been performed in *THOR*-knockdown H1299 cells [14], a lung cancer cell line, to identify downstream genes of *THOR*. However, no *THOR*-related transcriptome studies on the testicular tissue have yet been reported. This study generated the first RNA-seq dataset of *THOR*-knockout testes and age-matched control testes, offering a useful resource to investigate the physiological role of *THOR* in normal testis tissue, rather than in tumor tissues. Functional annotation and enrichment analysis on DEGs identified in this study suggest a probable role of *THOR* in cell cycle regulation within zebrafish testes. Specifically, we noticed the significant upregulation of several cell cycle-related genes, including *cdkn1d*, *foxo1a*, *tsc1a*, and *tsc2* in *THOR*-knockout testes. *cdkn1d* is a cyclin-dependent kinase inhibitor and its upregulation may induce cell cycle arrest [41]. *foxo1a* has been reported to inhibit cell cycle by enhancing the expression of cyclin-dependent kinase inhibitors and downregulating cyclin-dependent kinases [42, 43]. *tsc1a* and *tsc2* are the core components of the tuberous sclerosis complex (TSC) complex, which inhibits mechanistic target of rapamycin (mTOR) activity and thereby suppresses the G1/S transition [44, 45]. Collectively, upregulation of these genes implies a partial inhibition of the cell cycle in *THOR*-knockout testes, which was further experimentally supported by the reduction of pH 3 positive cells in the *THOR* knockout testes.

Apart from the aforementioned cell cycle inhibitors in upregulated DEGs, we also identified some intriguing downregulated genes, such as *atrx* and *rad21b*, in the *THOR*-knockout zebrafish testes. Atrx is an adenosine triphosphate (ATP)-dependent chromatin remodeler belonging to the SWItch (SWI)/Sucrose Non-Fermentable (SNF) family, which plays crucial roles in DNA replication, DNA repair, and maintenance of genomic stability [46, 47]. Atrx loss has been reported to result in a marked reduction of checkpoint kinase 1, leading to dysregulation of cell-cycle phase transition [48]. Conditional knockout of *Atrx* in mice leads to smaller testes with a range of spermatogenesis defects, due to prolonged G2/M phase and cell apoptosis [49]. As a core component of the cohesin complex, Rad21 is essential for homologous chromosome pairing and segregation during mitosis and meiosis [50, 51], and is also involved in DNA replication and homologous recombination repair of DNA double-strand breaks [52]. The remarkable downregulation of *atrx* and *rad21b* in *THOR*-knockout testes suggests that *THOR* may play an important regulatory role in DNA replication and DNA repair. Considering the fact that *THOR* was originally identified as a highly expressed lncRNA in various tumor cells [14, 15], it is not entirely unexpected that *THOR* knockout leads to aberrant expression of these mitosis- and DNA repair-related genes. Further studies are needed to explore the detailed roles and underlying mechanisms of *THOR*-mediated mitotic regulation during the normal process of spermatogenesis.

Long non-coding RNA *THOR* has been reported to interact with multiple proteins, such as IGF2BP1 and hnRNPD, to exert a promoting effect in tumorigenesis [14, 16, 18]. However, the interacting proteins of *THOR* in testicular tissue had not been systematically identified. In this study, by combining RNA pulldown with LC–MS/MS, we generated the first *THOR* interactome in zebrafish testes, which provides a new perspective for investigating its regulatory mechanisms in the testis. Functional annotation of the identified *THOR*-interacting proteins reveals potential roles of *THOR* in regulating RNA splicing, ribosome biogenesis, and chromatin architecture, all of which have been reported to be closely associated with spermatogenesis [53–56]. Most strikingly, the key components of the synaptonemal complex, Sycp1, Sycp2, and Sycp3, which are indispensable for spermatogenesis in zebrafish [57–59], were all identified to potentially interact with *THOR*. Moreover, the interaction between *THOR* and Sycp3 was further validated by endogenous and exogenous RIP assays, and the biological significance of this interaction was also explored in this study. Our experimental data showed that *THOR* overexpression significantly increased Sycp3 protein levels in a dose-dependent manner, whereas knockout of *THOR* in zebrafish testes significantly reduced Sycp3 protein levels and caused a discontinuous distribution of Sycp3 along paired chromosomes. Taken together, our study reveals a functional association between *THOR* and Sycp3, and supports the idea that *THOR* positively regulates Sycp3 protein levels to maintain meiotic progression in the zebrafish testis.

There are also some limitations in this study. Firstly, in vivo rescue experiments, such as *THOR* re-expression or Sycp3 overexpression in the $THOR^{-/-}$ zebrafish, have not been completed within this study, due to significant technical challenges and the extremely long experimental period. These experiments would strongly support the causality between the *THOR*-Sycp3 regulatory axis and the spermatogenesis defects. Secondly, this study primarily focuses on the identification and functional analysis of *THOR*-interacting proteins in the zebrafish testis. However, as a lncRNA, *THOR* may also exert regulatory functions by binding to DNA or RNA molecules. For example, our RNA-seq analysis revealed significant changes in the expression of mitosis- and DNA repair-related genes in *THOR* knockout testes, which may result from *THOR* regulating transcription via chromatin binding or modulating post-transcriptional RNA processing via RNA binding. Further studies may reveal novel functions and regulatory mechanisms of *THOR* in addition to the *THOR*-Sycp3 regulatory axis. These insights may be applicable not only to testicular tissues but also to tumor tissues.

In summary, we have characterized the testicular phenotype of *THOR*-knockout zebrafish. Loss of *THOR* impairs spermatogenesis, leading to reduced sperm number and motility, without affecting sex determination or gross testicular development. Mechanistically, *THOR* deficiency primarily dysregulates genes involved in cell cycle control and DNA repair. Moreover, *THOR* directly interacts with Sycp3 and promotes meiotic progression by stabilizing Sycp3 protein levels. These findings uncover a distinct role for *THOR* in spermatogenesis, separate from its oncogenic functions. They also provide a foundation for investigating broader activities of *THOR*—such as in cell cycle regulation, DNA replication and repair, RNA splicing, and ribosome biogenesis—and may inform future therapeutic strategies for male infertility and cancer.

Acknowledgment

We thank Prof. Meng Lu (Institute of Hydrobiology, Chinese Academy of Sciences) for his assistance with the chromosome spreading immunofluorescence assay. We are grateful to Fang Zhou, Guangxin Wang, and Xiaobing Dong (Analysis and Testing Center, Institute of Hydrobiology, Chinese Academy of Sciences) for helps in fluorescence image acquisition; Zhenfei Xing and Yuan Xiao (Analysis and Testing

Center, Institute of Hydrobiology, Chinese Academy of Sciences) for helps in scanning electron microscopy analysis; Min Wang (Analysis and Testing Center, Institute of Hydrobiology, Chinese Academy of Sciences) for helps in LC–MS/MS analysis.

Author contributions

J. Z.: Methodology, Formal analysis, Investigation, Writing—Original Draft, Visualization. C. J.: Methodology, Formal analysis, Investigation, Visualization. Y. L.: Formal analysis, Visualization. X. L.: Formal analysis, Visualization. Y. B.: Methodology, Resources. K. M.: Validation, Resources. Y. Z.: Validation, Data Curation. F. L.: Conceptualization, Methodology, Writing—Review & Editing, Supervision, Project administration. D. L.: Conceptualization, Writing—Review & Editing, Supervision, Project administration, Funding acquisition.

Supplementary data

Supplementary data are available at *BIOLRE* online.

Conflict of Interest: The authors declare no conflicts of interest.

Data availability

The RNA-seq raw data for WT and *THOR*$^{-/-}$ zebrafish testes are available in the (Genome Sequence Archive in National Genomics Data Center, China National Center for Bioinformation) at (https://ngdc.cncb.ac.cn/gsa), and can be accessed with the accession number (CRA038834). The human and mouse testis scRNA-seq data were downloaded from the NCBI GEO databases (https://www.ncbi.nlm.nih.gov/geo/) under accession numbers GSE149512 and GSE112393. Other data and information underlying this article will be shared on reasonable request to the corresponding authors.

References

1. Eisenberg ML, Esteves SC, Lamb DJ, Hotaling JM, Giwercman A, Hwang K, Cheng Y-S. Male infertility. *Nat Rev Dis Primers* 2023; **9**:49.
2. Nishimura H, L'Hernault SW. Spermatogenesis. *Curr Biol* 2017; **27**:R988–R994. https://doi.org/10.1016/j.cub.2017.07.067.
3. Cheng CY. Novel concepts of molecular mechanisms in spermatogenesis. *Semin Cell Dev Biol* 2022; **121**:1. https://doi.org/10.1016/j.semcdb.2021.08.005.
4. James ER, Tasnim M, Riera-Escamilla A, Vigh-Conrad K, Emery BR, Conrad DF, Aston KI. Genetic and epigenetic landscape of male infertility. *Trends Genet* 2025; **41**:883–898. https://doi.org/10.1016/j.tig.2025.07.007.
5. Hezroni H, Koppstein D, Matthew GS, Avrutin A, David PB, Ulitsky I. Principles of long noncoding RNA evolution derived from direct comparison of transcriptomes in 17 species. *Cell Rep* 2015; **11**:1110–1122. https://doi.org/10.1016/j.celrep.2015.04.023.
6. Washietl S, Kellis M, Garber M. Evolutionary dynamics and tissue specificity of human long noncoding RNAs in six mammals. *Genome Res* 2014; **24**:616–628. https://doi.org/10.1101/gr.165035.113.
7. Joshi M, Rajender S. Long non-coding RNAs (lncRNAs) in spermatogenesis and male infertility. *Reprod Biol Endocrinol* 2020; **18**:103.
8. Tzur YB. lncRNAs in fertility: redefining the gene expression paradigm? *Trends Genet* 2022; **38**:1170–1179. https://doi.org/10.1016/j.tig.2022.05.013.
9. Sahlu BW, Zhao S, Wang X, Umer S, Zou H, Huang J, Zhu H. Long noncoding RNAs: new insights in modulating mammalian spermatogenesis. *J Anim Sci Biotechnol* 2020; **11**:16.
10. Lu S, Li Y, Li C, Zou Z, Xu X, Zhu S, Yang B, Tang G, Chen H, Wang Y, Li F, Qin N, *et al.* Male specific conserved LncRNA TSCL1 regulated target mRNA translation by interaction with PIWIL1. *Cell Death Differ* 2026; **33**:411–427. https://doi.org/10.1038/s41418-025-01583-8.
11. Shao Z, Hu J, Jandura A, Wilk R, Jachimowicz M, Ma L, Hu C, Sundquist A, Das I, Samuel-Larbi P, Brill JA, Krause HM. Spatially revealed roles for lncRNAs in drosophila spermatogenesis, Y chromosome function and evolution. *Nat Commun* 2024; **15**:3806.
12. Reddy HM, Bhattacharya R, Tiwari S, Mishra K, Annapurna P, Jehan Z, Praveena NM, Alex JL, Dhople VM, Singh L, Sivaramakrishnan M, Chaturvedi A, *et al.* Y chromosomal noncoding RNAs regulate autosomal gene expression via piRNAs in mouse testis. *BMC Biol* 2021; **19**:198.
13. Lewandowski JP, Dumbović G, Watson AR, Hwang T, Jacobs-Palmer E, Chang N, Much C, Turner KM, Kirby C, Rubinstein ND, Groff AF, Liapis SC, *et al.* The Tug1 lncRNA locus is essential for male fertility. *Genome Biol* 2020; **21**:237.
14. Hosono Y, Niknafs YS, Prensner JR, Iyer MK, Dhanasekaran SM, Mehra R, Pitchiaya S, Tien J, Escara-Wilke J, Poliakov A, Chu S-C, Saleh S, *et al.* Oncogenic role of THOR, a conserved cancer/testis long non-coding RNA. *Cell* 2017; **171**:1559–1572.e1520. https://doi.org/10.1016/j.cell.2017.11.040.
15. Chong ZX. Unleashing lncRNA THOR: roles in cancer progression and clinical outlook. *Mol Genet Genom* 2026; **301**:75.
16. Hu H, Zhang H, Xing Y, Zhou Y, Chen J, Li C, Xu J, Guo Y, Wang J, He Q, Liu X, Sheng J, *et al.* The lncRNA THOR interacts with and stabilizes hnRNPD to promote cell proliferation and metastasis in breast cancer. *Oncogene* 2022; **41**:5298–5314. https://doi.org/10.1038/s41388-022-02495-4.
17. Xue J, Zhong S, Sun BM, Sun QF, Hu LY, Pan SJ. Lnc-THOR silencing inhibits human glioma cell survival by activating MAGEA6-AMPK signaling. *Cell Death Dis* 2019; **10**:866.
18. Wang SS, Lv Y, Xu XC, Zuo Y, Song Y, Wu GP, Lu PH, Zhang ZQ, Chen MB. Triptonide inhibits human nasopharyngeal carcinoma cell growth via disrupting Lnc-RNA THOR-IGF2BP1 signaling. *Cancer Lett* 2019; **443**:13–24. https://doi.org/10.1016/j.canlet.2018.11.028.
19. Song H, Xu Y, Shi L, Xu T, Fan R, Cao M, Xu W, Song J. LncRNA THOR increases the stemness of gastric cancer cells via enhancing SOX9 mRNA stability. *Biomed Pharmacother* 2018; **108**:338–346. https://doi.org/10.1016/j.biopha.2018.09.057.
20. Gao L, Cheng X-L, Cao H. LncRNA THOR attenuates cisplatin sensitivity of nasopharyngeal carcinoma cells via enhancing cells stemness. *Biochimie* 2018; **152**:63–72. https://doi.org/10.1016/j.biochi.2018.06.015.
21. Cheng Z, Lei Z, Yang P, Si A, Xiang D, Zhou J, Hüser N. Long non-coding RNA THOR promotes liver cancer stem cells expansion via β-catenin pathway. *Gene* 2019; **684**:95–103. https://doi.org/10.1016/j.gene.2018.10.051.
22. Wang B, Ye Q, Zou C. Long non-coding RNA THOR enhances the stem cell-like traits of triple-negative breast cancer cells through activating β-catenin signaling. *Med Sci Monit* 2020; **26**:e923507. https://doi.org/10.12659/MSM.923507.
23. Zhou L, Li J, Liu J, Wang A, Liu Y, Yu H, Ouyang H, Pang D. Investigation of the lncRNA THOR in mice highlights the importance of noncoding RNAs in mammalian male reproduction. *Biomedicines* 2021; **9**:859. https://doi.org/10.3390/biomedicines9080859.
24. Liu F, Qin Y, Huang Y, Gao P, Li J, Yu S, Jia D, Chen X, Lv Y, Tu J, Sun K, Han Y, *et al.* Rod genesis driven by mafba in an nrl knockout zebrafish model with altered photoreceptor composition and progressive retinal degeneration. *PLoS Genet* 2022; **18**:e1009841. https://doi.org/10.1371/journal.pgen.1009841.
25. Liu F, Qin Y, Yu S, Soares DC, Yang L, Weng J, Li C, Gao M, Lu Z, Hu X, Liu X, Jiang T, *et al.* Pathogenic mutations in retinitis pigmentosa 2 predominantly result in loss of RP2 protein stability in humans and zebrafish. *J Biol Chem* 2017; **292**:6225–6239. https://doi.org/10.1074/jbc.M116.760314.
26. Ye D, Liu T, Li YM, Wang YP, Hu W, Zhu ZY, Sun YH. Identification of fish spermatogenic cells through high-throughput immunofluorescence against testis with an antibody

set. *Front Endocrinol* 2023; **14**:1044318. https://doi.org/10.3389/fendo.2023.1044318.
27. Miao LJ, Zhou L, Chen Y, Li Z, Han X, Peng F, Yang L, Li YD, Zhang XJ, Lu M, Wang ZW, Li XY, *et al.* Mei4 deficiency induces sexual dimorphism in early meiosis and promotes production of unreduced eggs in zebrafish. *Zool Res* 2026; **47**:547–560. https://doi.org/10.24272/j.issn.2095-8137.2025.186.
28. Choi HMT, Schwarzkopf M, Fornace ME, Acharya A, Artavanis G, Stegmaier J, Cunha A, Pierce NA. Third-generation in situ hybridization chain reaction: multiplexed, quantitative, sensitive, versatile, robust. *Development* 2018; **145**:dev165753. https://doi.org/10.1242/dev.165753.
29. Lin X, Zhao Y, Bai Y, Meng K, Chen Y, Hu M, Liu F, Luo D. Integrating gonadal RNA-seq and small RNA-seq to analyze mRNA and miRNA changes in medaka sex differentiation. *Sci Data* 2025; **12**:778.
30. Chen Y, Lin X, Dai J, Bai Y, Liu F, Luo D. Deletion of ddx4 ovary-specific transcript causes dysfunction of meiosis and derepress of DNA transposons in zebrafish ovaries. *Biology* 2024; **13**:1055. https://doi.org/10.3390/biology13121055.
31. Peritz T, Zeng F, Kannanayakal TJ, Kilk K, Eiriksdottir E, Langel U, Eberwine J. Immunoprecipitation of mRNA-protein complexes. *Nat Protoc* 2006; **1**:577–580. https://doi.org/10.1038/nprot.2006.82.
32. Zhao L, Yao C, Xing X, Jing T, Li P, Zhu Z, Yang C, Zhai J, Tian R, Chen H, Luo J, Liu N, *et al.* Single-cell analysis of developing and azoospermia human testicles reveals central role of Sertoli cells. *Nat Commun* 2020; **11**:5683. https://doi.org/10.1038/s41467-020-19414-4.
33. Green CD, Ma Q, Manske GL, Shami AN, Zheng X, Marini S, Moritz L, Sultan C, Gurczynski SJ, Moore BB, Tallquist MD, Li JZ, *et al.* A comprehensive roadmap of murine spermatogenesis defined by single-cell RNA-Seq. *Dev Cell* 2018; **46**:651–667.e10. https://doi.org/10.1016/j.devcel.2018.07.025.
34. Qian P, Kang J, Liu D, Xie G. Single cell transcriptome sequencing of zebrafish testis revealed novel spermatogenesis marker genes and stronger Leydig-germ cell paracrine interactions. *Front Genet* 2022; **13**:851719. https://doi.org/10.3389/fgene.2022.851719.
35. Haimbaugh A, Akemann C, Meyer D, Gurdziel K, Baker TR. Insight into 2,3,7,8-tetrachlorodibenzo-p-dioxin-induced disruption of zebrafish spermatogenesis via single cell RNA-seq. *PNAS Nexus* 2022;**1**:pgac060. https://doi.org/10.1093/pnasnexus/pgac060.
36. Adams IR, Davies OR. Meiotic chromosome structure, the synaptonemal complex, and infertility. *Annu Rev Genomics Hum Genet* 2023; **24**:35–61. https://doi.org/10.1146/annurev-genom-110122-090239.
37. Cesar BI, Kim Y. Structure and function of the synaptonemal complex. *J Cell Biol* 2026; **225**:e202511222. https://doi.org/10.1083/jcb.202511222.
38. Liu H, Xu Y, Yao B, Sui T, Lai L, Li Z. A novel N6-methyladenosine (m6A)-dependent fate decision for the lncRNA THOR. *Cell Death Dis* 2020; **11**:613.
39. Ge J, Han T, Shan L, Na J, Li Y, Wang J. Long non-coding RNA THOR promotes ovarian cancer cells progression via IL-6/STAT3 pathway. *J Ovarian Res* 2020; **13**:72.
40. Jiao P-F, Tang P-J, Chu D, Li Y-M, Xu W-H, Ren G-F. Long non-coding RNA THOR depletion inhibits human non-small cell lung cancer cell growth. *Front Oncol* 2021; **11**:756148.
41. Laranjeiro R, Tamai TK, Peyric E, Krusche P, Ott S, Whitmore D. Cyclin-dependent kinase inhibitor p20 controls circadian cell-cycle timing. *Proc Natl Acad Sci U S A* 2013; **110**:6835–6840. https://doi.org/10.1073/pnas.1217912110.
42. Schmidt M, de Mattos SF, van der Horst A, Klompmaker R, Kops GJPL, Lam EWF, Burgering BMT, Medema RH. Cell cycle inhibition by FoxO forkhead transcription factors involves down-regulation of cyclin D. *Mol Cell Biol* 2002; **22**:7842–7852. https://doi.org/10.1128/MCB.22.22.7842-7852.2002.
43. Reagan-Shaw S, Ahmad N. RNA interference-mediated depletion of phosphoinositide 3-kinase activates Forkhead box class O transcription factors and induces cell cycle arrest and apoptosis in breast carcinoma cells. *Cancer Res* 2006; **66**:1062–1069. https://doi.org/10.1158/0008-5472.CAN-05-1018.
44. Cuyàs E, Corominas-Faja B, Joven J, Menendez JA. Cell cycle regulation by the nutrient-sensing mammalian target of rapamycin (mTOR) pathway. *Methods Mol Biol* 2014; **1170**:113–144.
45. Joshi JN, Lerner AD, Scallo F, Grumet AN, Matteson P, Millonig JH, Valvezan AJ. mTORC1 activity oscillates throughout the cell cycle, promoting mitotic entry and differentially influencing autophagy induction. *Cell Rep* 2024; **43**:114543. https://doi.org/10.1016/j.celrep.2024.114543.
46. Aguilera P, López-Contreras AJ. ATRX, a guardian of chromatin. *Trends Genet* 2023; **39**:505–519. https://doi.org/10.1016/j.tig.2023.02.009.
47. Juhász S, Elbakry A, Mathes A, Löbrich M. ATRX promotes DNA repair synthesis and sister chromatid exchange during homologous recombination. *Mol Cell* 2018; **71**:11–24.e7. https://doi.org/10.1016/j.molcel.2018.05.014.
48. Qin T, Mullan B, Ravindran R, Messinger D, Siada R, Cummings JR, Harris M, Muruganand A, Pyaram K, Miklja Z, Reiber M, Garcia T, *et al.* ATRX loss in glioma results in dysregulation of cell-cycle phase transition and ATM inhibitor radiosensitization. *Cell Rep* 2022; **38**:110216. https://doi.org/10.1016/j.celrep.2021.110216.
49. Bagheri-Fam S, Argentaro A, Svingen T, Combes AN, Sinclair AH, Koopman P, Harley VR. Defective survival of proliferating Sertoli cells and androgen receptor function in a mouse model of the ATR-X syndrome. *Hum Mol Genet* 2011; **20**:2213–2224. https://doi.org/10.1093/hmg/ddr109.
50. Sun Y, Xu X, Zhao W, Zhang Y, Chen K, Li Y, Wang X, Zhang M, Xue B, Yu W, Hou Y, Wang C, *et al.* RAD21 is the core subunit of the cohesin complex involved in directing genome organization. *Genome Biol* 2023; **24**:155.
51. Urban E, Nagarkar-Jaiswal S, Lehner CF, Heidmann SK. The cohesin subunit Rad21 is required for synaptonemal complex maintenance, but not sister chromatid cohesion, during drosophila female meiosis. *PLoS Genet* 2014; **10**:e1004540. https://doi.org/10.1371/journal.pgen.1004540.
52. Di Nardo M, Pallotta MM, Musio A. The multifaceted roles of cohesin in cancer. *J Exp Clin Cancer Res* 2022; **41**:96.
53. Song H, Wang L, Chen D, Li F. The function of pre-mRNA alternative splicing in mammal spermatogenesis. *Int J Biol Sci* 2020; **16**:38–48. https://doi.org/10.7150/ijbs.34422.
54. Jiang L, Li T, Zhang X, Zhang B, Yu C, Li Y, Fan S, Jiang X, Khan T, Hao Q, Xu P, Nadano D, *et al.* RPL10L is required for male meiotic division by compensating for RPL10 during meiotic sex chromosome inactivation in mice. *Curr Biol* 2017; **27**:1498–1505.e6. https://doi.org/10.1016/j.cub.2017.04.017.
55. Zou Q, Yang L, Shi R, Qi Y, Zhang X, Qi H. Proteostasis regulated by testis-specific ribosomal protein RPL39L maintains mouse spermatogenesis. *iScience* 2021; **24**:103396. https://doi.org/10.1016/j.isci.2021.103396.
56. Wang Y, Wang H, Zhang Y, Du Z, Si W, Fan S, Qin D, Wang M, Duan Y, Li L, Jiao Y, Li Y, *et al.* Reprogramming of meiotic chromatin architecture during spermatogenesis. *Mol Cell* 2019; **73**:547–561.e6. https://doi.org/10.1016/j.molcel.2018.11.019.
57. Olaya I, Yilmaz IN, Nour-Kasally N, Charboneau RE, Draper BW, Burgess SM. Distinct cellular and reproductive consequences of meiotic chromosome synapsis defects in syce2 and sycp1 mutant zebrafish. *PLoS Genet* 2025; **21**:e1011656. https://doi.org/10.1371/journal.pgen.1011656.

58. Takemoto K, Imai Y, Saito K, Kawasaki T, Carlton PM, Ishiguro K-ı, Sakai N. Sycp2 is essential for synaptonemal complex assembly, early meiotic recombination and homologous pairing in zebrafish spermatocytes. *PLoS Genet* 2020; **16**:e1008640. https://doi.org/10.1371/journal.pgen.1008640.

59. Pan Y-J, Tong S-K, Hsu C-w, Weng J-H, Chung B-c. Zebrafish establish female germ cell identity by advancing cell proliferation and meiosis. *Front Cell Dev Biol* 2022; **10**:866267. https://doi.org/10.3389/fcell.2022.866267.

© The Author(s) 2026. Published by Oxford University Press on behalf of the Society for the Study of Reproduction. This is an Open Access article distributed under the terms of the Creative Commons Attribution-NonCommercial License (https://creativecommons.org/licenses/by-nc/4.0/), which permits non-commercial re-use, distribution, and reproduction in any medium, provided the original work is properly cited. For commercial re-use, please contact reprints@oup.com for reprints and translation rights for reprints. All other permissions can be obtained through our RightsLink service via the Permissions link on the article page on our site—for further information please contact journals.permissions@oup.com.
Biology of Reproduction, 2026, 115(4), 1331–1350
https://doi.org/10.1093/biolre/ioag185
Research Article